AVP-induced counter-regulatory glucagon is diminished in type 1 diabetes

Angela Kim[1,2], Jakob G. Knudsen[3,4], Joseph C. Madara[1], Anna Benrick[5], Thomas Hill[3], Lina Abdul Kadir[3], Joely A. Kellard[3], Lisa Mellander[5], Caroline Miranda[5], Haopeng Lin[6], Timothy James[7], Kinga Suba[8], Aliya F. Spigelman[6], Yanling Wu[5], Patrick E. MacDonald[6], Ingrid Wernstedt Asterholm[5], Tore Magnussen[9], Mikkel Christensen[9,10,11], Tina Vilsboll[9,10,12], Victoria Salem[8], Filip K. Knop[9,10,12,13], Patrik Rorsman[3,5], Bradford B. Lowell[1,2], Linford J.B. Briant[3,14,*]

Affiliations

[1]Division of Endocrinology, Diabetes, and Metabolism, Beth Israel Deaconess Medical Center, Boston, MA 02215, USA. [2]Program in Neuroscience, Harvard Medical School, Boston, MA 02115, USA. [3]Oxford Centre for Diabetes, Endocrinology and Metabolism, Radcliffe Department of Medicine, University of Oxford, Oxford, OX4 7LE, UK. [4]Section for Cell Biology and Physiology, Department of Biology, University of Copenhagen. [5]Institute of Neuroscience and Physiology, Metabolic Research Unit, University of Göteborg, 405 30, Göteborg, Sweden. [6]Alberta Diabetes Institute, 6-126 Li Ka Shing Centre for Health Research Innovation, Edmonton, Alberta, T6G 2E1, Canada. [7]Department of Clinical Biochemistry, John Radcliffe, Oxford NHS Trust, OX3 9DU, Oxford, UK. [8]Section of Cell Biology and Functional Genomics, Department of Metabolism, Digestion and Reproduction, Imperial College London, W12 0NN, UK. [9]Center for Clinical Metabolic Research, Gentofte Hospital, Kildegårdsvej 28, DK-2900 Hellerup, Denmark. [10]Department of Clinical Pharmacology, Bispebjerg Hospital, University of Copenhagen, DK-2400 Copenhagen,

[11]Department of Clinical Medicine, Faculty of Health and Medical Sciences, University of Copenhagen, Copenhagen, Denmark. [12]Steno Diabetes Center Copenhagen, DK-2820 Gentofte, Copenhagen, Denmark. [13]Novo Nordisk Foundation Center for Basic Metabolic Research, Faculty of Health and Medical Sciences, University of Copenhagen, Copenhagen, Denmark.[14]Department of Computer Science, University of Oxford, Oxford, OX1 3QD, UK.

*Corresponding author: Linford J.B. Briant, linford.briant@ocdem.ox.ac.uk

Abstract

Hypoglycaemia is a major barrier to the treatment of diabetes. Accordingly, it is important that we understand the mechanisms regulating the circulating levels of glucagon – the body's principle blood glucose-elevating hormone which is secreted from alpha-cells of the pancreatic islets. In isolated islets, varying glucose over the range of concentrations that occur physiologically between the fed and fuel-deprived states (from 8 to 4 mM) has no significant effect on glucagon secretion and yet associates with dramatic changes in plasma glucagon *in vivo*. The identity of the systemic factor that stimulates glucagon secretion *in vivo* remains unknown. Here, we show that arginine-vasopressin (AVP), secreted from the posterior pituitary, stimulates glucagon secretion. Glucagon-secreting alpha-cells express high levels of the vasopressin 1b receptor (V1bR). Activation of AVP neurons *in vivo* increased circulating AVP, stimulated glucagon release and evoked hyperglycaemia; effects blocked by pharmacological antagonism of either the glucagon receptor or vasopressin 1b receptor. AVP also mediates the stimulatory effects of dehydration and hypoglycaemia produced by exogenous insulin and 2-deoxy-D-glucose on glucagon secretion. We show that the A1/C1 neurons of the medulla oblongata, which are known to be activated by hypoglycaemia, drive AVP neuron activation in response to insulin-induced hypoglycaemia. Hypoglycaemia also increases circulating levels of copeptin (derived from the same pre-pro hormone as AVP) in humans and this hormone stimulates glucagon secretion from isolated human islets. In patients with type 1 diabetes, hypoglycaemia failed to increase both plasma copeptin and glucagon. These findings provide a new mechanism for the central regulation of glucagon secretion in both health and disease.

Introduction

A tight regulation of blood glucose is critical for normal brain function. For this reason, hypoglycaemia evokes a multitude of responses to counter deleterious declines in blood glucose and avert brain failure and ultimately death (Cryer, 2007). A critical component to this "counter-regulatory" response is the elevation of plasma glucagon - a hormone that is considered the first line of defence against hypoglycaemia (Cryer, 1994).

Glucagon is secreted from alpha-cells of the pancreatic islets, and counters hypoglycaemia by potently stimulating hepatic glucose production. The importance of glucagon for glucose homeostasis is demonstrated in both type 1 and type 2 diabetes mellitus, wherein hyperglycaemia results from a combination of complete/partial loss of insulin secretion and over-secretion of glucagon (Unger & Cherrington, 2012). Despite the centrality of glucagon to diabetes aetiology and its importance in countering hypoglycaemia, there remains considerable uncertainty regarding how its secretion is regulated.

The mechanism(s) by which glucagon secretion is controlled is a contentious topic (Gylfe, 2013; Lai *et al.*, 2018). Based on observations in isolated (*ex vivo*) islets, islets have been shown to respond to hypoglycaemia (and adjust glucagon secretion accordingly) via intrinsic (Rorsman *et al.*, 2014; Basco *et al.*, 2018; Yu *et al.*, 2019) and paracrine mechanisms (Briant *et al.*, 2018; Vergari *et al.*, 2019). While it is indisputable that the islet is a critical component of the body's glucostat (Rodriguez-Diaz *et al.*, 2018) and has the ability to intrinsically modulate glucagon output, it is clear that such an 'islet-centric' viewpoint is overly simplistic (Schwartz *et al.*, 2013). Indeed, many studies have clearly demonstrated that brain-directed interventions can profoundly alter islet alpha-cell function, with glucose-sensing neurons in the hypothalamus being key mediators (Garfield *et al.*, 2014; Lamy *et al.*, 2014; Meek *et al.*,

2016). This ability of the brain to modulate glucagon secretion is commonly attributed to autonomic innervation of the pancreas (Marty *et al.*, 2005; Lamy *et al.*, 2014; Thorens, 2014). However, counter-regulatory glucagon secretion is not only restored in pancreas transplant patients but also insensitive to adrenergic blockade (Diem *et al.*, 1990), suggesting that other (non-autonomic) central mechanisms may also contribute to counter-regulatory glucagon secretion *in vivo*.

Arginine-vasopressin (AVP) is a hormone synthesised in the hypothalamus (see review by Bourque (2008)). AVP neurones are divided into two classes: parvocellular AVP neurons (which either project to the median eminence to stimulate ACTH and glucocorticoid release or project centrally to other brain regions) and magnocellular AVP neurons (which are the main contributors to circulating levels of AVP). The parvocellular neurones reside solely in the paraventricular nucleus of the hypothalamus (PVH), whereas magnocellular neurones are found in both the PVH and supraoptic nucleus (SON). Stimulation of the magnocellular AVP neurons causes release of AVP into the posterior pituitary, where it enters the peripheral circulation.

Animals that have had glucagon signalling blocked with an antibody against the glucagon receptor exhibit profound hyperglucagonaemia (Sloop *et al.*, 2004). In these mice, transcripts for the vasopressin 1b receptor (*Avpr1b*) are highly upregulated in alpha-cells (Kim *et al.*, 2017). Even under normal conditions, *Avpr1b* is one of the most enriched transcripts in alpha-cells (Lawlor *et al.*, 2017; van der Meulen *et al.*, 2017). This raises the possibility that AVP may be an important regulator of glucagon secretion under physiological conditions and that this regulatory pathway is utilised in conditions of interrupted glucagon signalling to bolster glucagon output. Here, we have investigated the regulation of glucagon by circulating AVP.

We show that glucagon secretion in response to hypoglycaemia is due to AVP and we identify a novel role for glucagon; maintaining plasma glucose in the dehydrated state. Finally, we explore the link between copeptin (co-secreted with AVP but with a longer circulating half-life) and glucagon in humans and provide evidence that this pituitary-alpha-cell axis is impaired in type 1 diabetes.

Results

Glucagon secretion in response to an insulin tolerance test is driven by AVP

Hypoglycaemia induced by an insulin tolerance test (ITT) robustly stimulates glucagon secretion *in vivo* (Fig. 1a, b). However, reducing the glucose concentration from 8 to 4 mM (mimicking an ITT) does not stimulate glucagon secretion from isolated (*ex vivo*) islets (Fig. 1c). Therefore, mechanisms extrinsic to the islet must control glucagon secretion *in vivo*, at least during an ITT. We hypothesised that this extrinsic stimulus is AVP. First, we investigated whether AVP neuron activity is increased in response to an ITT *in vivo* using fibre photometry (Fig. 1d-h). Exogenous insulin evoked an increase in AVP neuron activity (Fig. 1f-h), whereas saline vehicle treatment was ineffective (Fig. 1f-h). Finally, we confirmed that plasma AVP is elevated following an ITT by measuring its surrogate marker, copeptin (the C-terminal fragment of pre-pro-AVP; Fig. 1i).

To investigate the kinetics and glucose-dependency of this response, we simultaneously recorded AVP neuron activity and plasma glucose (by continuous glucose monitoring; Fig. 2a, b). This revealed that AVP neuron activity initiates at 4.9 ±0.4 mM glucose (Fig. 2c) at a delay of ~10 mins (Fig. 2d). Once the threshold was reached, AVP neurons displayed random bursts of activity. The amount of AVP neuronal activation did not correlate with the extent of hypoglycemia. Neither frequency nor peak amplitude correlated with the blood glucose change. Insulin-induced hypoglycemia was accompanied by a significant decrease in the body temperature (Fig. 2e), as previously reported (Freinkel *et al.*, 1972; Buchanan *et al.*, 1991).

To determine whether AVP contributes to glucagon secretion during an insulin-induced hypoglycaemia, we injected wild-type mice with the V1bR antagonist SSR149415

(nelivaptan; Serradeil-Le Gal *et al.* (2002)) prior to the ITT (Fig. 3a-b). This reduced insulin-induced glucagon secretion by 70%. Similarly, in *Avpr1b* knockout mice (*Avpr1b*$^{-/-}$; Lolait *et al.* (2007)) glucagon secretion was decreased by 65% compared to wild-type littermates (*Avpr1b*$^{-/-}$; Fig. 3c-d). There was not a change in the depth of hypoglycaemia induced following V1bR antagonism (Fig. 3b) or in *Avpr1b*$^{-/-}$ mice (Fig. 3d), despite the drastic reduction in plasma glucagon. Thus, it appears that the supraphysiological concentrations of insulin likely dominate the hyperglycaemic action of endogenous glucagon. This 'glucagonostatic' effect of *Avpr1b* antagonism or KO was also observed during deeper hypoglycaemia, achieved with a higher dose of insulin (Fig. 3e-h).

AVP has also been reported to increase circulating corticosterone (Antoni, 1993) and adrenaline (Grazzini *et al.*, 1996), but in our experiments neither adrenaline (Supplementary Fig. 1a-c) nor corticosterone (Supplementary Fig. 1d and e) increased glucagon output or alpha-cell activity in isolated mouse or human islets.

We next investigated the role of AVP in controlling glucagon secretion evoked by 2-deoxy-D-glucose (2DG). 2DG is a non-metabolisable glucose molecule that evokes a state of perceived glucose deficit (mimicking hypoglycaemia) that triggers a robust counter-regulatory stimulation of glucagon secretion (Marty *et al.*, 2005). We hypothesised that AVP contributes to this response. We monitored AVP neuron activity in response to 2DG by *in vivo* fibre photometry (as per Fig. 1d), and correlated this to changes in plasma glucose during this metabolic challenge (Supplementary Fig. 2). Injection (i.p.) of 2DG increased blood glucose (Supplementary Fig. 2a) and triggered a concomitant elevation of GCaMP6s signal in AVP neurons (Supplementary Fig. 2b-d). The hyperglycaemic response to 2DG was suppressed by pre-treatment with either the V1bR antagonist SSR149415 or the glucagon

receptor antagonist LY2409021 (Supplementary Fig. 2e; Kazda *et al.* (2016)). Finally, the elevation in plasma glucagon by 2DG injection was reduced following pretreatment with the V1bR antagonist SSR149415 (Supplementary Fig. 2f). We conclude that AVP contributes to the hyperglycaemic response to 2DG by stimulating glucagon release.

AVP evokes hyperglycaemia and hyperglucagonaemia

Next, we investigated the mechanisms by which AVP stimulates glucagon during hypoglycaemia. We first investigated the metabolic effects of AVP *in vivo* (Fig. 4a-d). We expressed the modified human M3 muscarinic receptor hM3Dq (see Alexander *et al.* (2009)) in AVP neurons by bilaterally injecting a Cre-dependent virus containing hM3Dq (AAV-DIO-hM3Dq-mCherry) into the supraoptic nucleus (SON) of mice bearing *Avp* promoter-driven Cre recombinase (*Avp*$^{ires\text{-}Cre+}$ mice; Fig. 4a). Expression of hM3Dq was limited to the SON (Supplementary Fig. 3), thus allowing targeted activation of magnocellular AVP neurons (which determine circulating AVP). Patch-clamp recordings from brain slices of the SON prepared from these mice confirmed that bath application of clozapine-N-oxide (CNO; 5-10 µM) – a specific, pharmacologically inert agonist for hM3Dq - induced membrane depolarisation and increased the firing rate in hM3Dq-expressing AVP neurons (Supplementary Fig. 3a and b). Injection of CNO (3 mg/kg i.p.) *in vivo* increased blood glucose (Fig. 4b) and copeptin (Fig. 4c). To establish the contribution of glucagon to this hyperglycaemic response, we pre-treated mice with the glucagon receptor antagonist LY2409021. This completely abolished the hyperglycaemic action of CNO (Fig. 4b). Similarly, to understand the contribution of vasopressin 1b receptor (V1bR) signalling, we pre-treated mice with the V1bR antagonist SSR149415. This also abolished the hyperglycaemic effect of CNO (Fig. 4b). Measurements of plasma glucagon during CNO treatment revealed it was elevated by ~40% (Fig. 4d). We note that this response was modest,

which could reflect the variability in hM3Dq expression or the fact that the elevation in blood glucose exerts a glucagonostatic effect. CNO did not change food intake (Supplementary Fig. 3f) and did not have an off-target effect on blood glucose in *Avp*$^{ires\text{-}Cre+}$ mice expressing a passive protein (mCherry) under AAV transfection in the SON (Supplementary Fig. 3g). Exogenous AVP also caused an increase in glucose and glucagon relative to saline injection in wild-type mice (Supplementary Fig. 3h-j). In summary, CNO stimulates AVP release, which in turn elevates plasma glucose through stimulation of glucagon release.

To determine whether the hyperglycaemic and hyperglucagonaemic actions of AVP are due to AVP directly stimulating glucagon secretion from alpha-cells, we assessed the response of islets to AVP. First, we assessed this response *in vivo*; we isolated islets from *Gcg*$^{Cre+}$ mice crossed with a Cre-dependent GCaMP3 reporter mouse (from hereon, *Gcg*-GCaMP3 mice) and implanted them in the anterior chamber of the eye (Fig. 4e-h; see Salem *et al.* (2019)). This allows the cytoplasmic Ca^{2+} concentration ($[Ca^{2+}]_i$) in individual alpha-cells to be imaged *in vivo*. Administration (i.v.) of AVP resulted in a biphasic elevation of $[Ca^{2+}]_i$ consisting of an intial spike followed by rapid oscillatory activity (Fig. 4f-g).

To understand whether AVP stimulates glucagon secretion directly from islets, we made a detailed assessment of the response of isolated (*ex vivo*) mouse islets and the *in situ* perfused pancreas to AVP. First, we characterised the expression of vasopressin receptors in mouse islets. V1bR mRNA (*Avpr1b*) was expressed in whole mouse islets, whereas vasopressin receptor subtypes 1a and 2 mRNA were not; instead, they were detected in various extra-pancreatic tissue, consistent with their distinct roles in the regulation of blood pressure and diuresis (Bourque, 2008), respectively (Supplementary Fig. 4a). To determine whether *Avpr1b* expression was enriched in alpha-cells, mice bearing a proglucagon promoter-driven

Cre-recombinase (*Gcg*$^{Cre+}$ mice) were crossed with mice expressing a Cre-driven fluorescent reporter (RFP). qPCR of the fluorescence-activated cell sorted RFP^{+} and RFP^{-} fractions revealed that *Avpr1b* is upregulated in mouse alpha-cells with ~43-fold enrichment (Supplementary Fig. 4c and d).

AVP dose-dependently stimulated glucagon secretion from isolated mouse islets (Supplementary Fig. 5). In dynamic measurements using *in situ* perfused mouse pancreas, AVP was found to produce a biphasic increase in glucagon secretion (Supplementary Fig. 5d). In mouse islets, the AVP-induced increase in glucagon was prevented by SSR149415 (Supplementary Fig. 5c). AVP did not affect insulin secretion (Supplementary Fig. 5e-h). To understand the intracellular mechanisms by which AVP stimulates glucagon secretion, we performed perforated patch-clamp recordings of electrical activity and Ca^{2+} imaging in alpha-cells in isolated islets from *Gcg*$^{Cre+}$ mice crossed with a Cre-dependent GCaMP3 reporter mouse (from hereon, *Gcg*-GCaMP3 mice). AVP increased action potential firing (Supplementary Fig. 5i, j) and Ca^{2+} oscillations (Supplementary Fig. 5k, l) in a dose-dependent manner. The Ca^{2+} response was abolished following application of the V1bR antagonist SSR149415 (Supplementary Fig. 5m, n). AVP-induced Ca^{2+} activity was dependent on G_q-protein activation, because it was blocked with the G_q-inhibitor YM254890 (Takasaki *et al*. (2004); Supplementary Fig. 6a, b) and it increased intracellular diacylglycerol (Supplementary Fig. 6c, d). In line with G_q activation, electrical activity evoked by AVP exhibited membrane potential oscillations (as revealed by power-spectrum analysis; Supplementary Fig. 6e). Conducting mathematical modelling of the intracellular signalling pathway following G_q receptor activation demonstrated that the canonical G_q pathway can evoke Ca^{2+} oscillations, further supporting the involvement of VlbR, a G_q

protein-coupled receptor, in stimulating glucagon secretion from alpha cells (Supplementary Fig. 6f, g).

Hypoglycaemia evokes AVP secretion via activation of A1/C1 neurons

Many physiological stressors activate hindbrain catecholamine neurons, which release noradrenaline (A1) or adrenaline (C1) and reside in the ventrolateral portion of the medulla oblongata (VLM). Activation of C1 neurons (by targeted glucoprivation or chemogenetic manipulation) is known to elevate blood glucose (Ritter *et al.*, 2000; Zhao *et al.*, 2017; Li *et al.*, 2018) and plasma glucagon (Andrew *et al.*, 2007). Furthermore, C1 cell lesions severely attenuate the release of AVP in response to hydralazine-evoked hypotension (Madden *et al.*, 2006), indicating that this hindbrain site may be a key regulator of AVP neuron activity during physiological stress.

To characterize any functional connectivity between A1/C1 neurons and SON AVP neurons, we conducted channelrhodpsin-2-assisted circuit mapping (CRACM; Petreanu *et al.* (2007)) and viral tracer studies (Fig. 5a-e). We injected a Cre-dependent viral vector containing the light-gated ion channel channelrhodopsin-2 (AAV-DIO-ChR2-mCherry) into the VLM (targeting A1/C1 neurons) of Avp^{GFP} *x* Th^{Cre+} mice (Fig. 5a). Projections from the A1/C1 neurons were present in the SON and PVH and co-localised with AVP-immunoreactive neurons (Fig. 5b and Supplementary Fig. 7a). Brain slice electrophysiology revealed that in the majority (89%) of GFP^{+} AVP neurons, opto-activation of A1/C1 neuron terminals results in excitatory post-synaptic currents (EPSCs; Fig. 5c, d). These EPSCs were glutamatergic, as they were abolished by the AMPA and kainate receptor antagonist DNQX (Fig. 5c). Furthermore, these EPSCs could be blocked with TTX, but reinstated with addition of 4-AP

(Fig. 5e), indicating that A1/C1 neurones connect to AVP neurons in the SON monosynaptically.

To explore the consequences of A1/C1 activation *in vivo*, we injected AAV-DIO-hM3Dq-mCherry bilaterally into the VLM of Th^{Cre+} mice (Fig. 5f, Supplementary Fig. 7b, c). Activation of A1/C1 neurons with CNO evoked a ~4.5 mM increase in plasma glucose (Fig. 5g, h). Pre-treatment with the glucagon receptor antagonist LY2409021 inhibited this response (Fig. 5g, h). In line with this, plasma glucagon was increased following CNO application (Fig. 5i). The hyperglycaemic response was also dependent on functional V1bRs, because it was abolished following pre-treatment with the V1bR antagonist SSR149415 (Fig. 5g, h). CNO had no effect on blood glucose in Th^{Cre+} mice expressing mCherry in A1/C1 neurons (Supplementary Fig. 7c). Together, these data indicate that A1/C1 neuron activation evokes AVP and glucagon secretion. We therefore hypothesised that hypoglycaemia-induced AVP release is due to projections from A1/C1 neurons.

In line with this hypothesis, c-Fos expression (a marker of neuronal activity) was increased in A1/C1 neurons following an insulin bolus (Supplementary Fig. 8a and b).

To determine the contribution of A1/C1 neurons to AVP neuron activity during an ITT, we inhibited A1/C1 neurons whilst monitoring AVP neuron activity. To this end, we expressed an inhibitory receptor (the modified human muscarinic M4 receptor hM4Di; Armbruster *et al.* (2007)) in A1/C1 neurons by injecting AAV-fDIO-hM4Di-mCherry into the VLM, whilst co-injecting AAV-DIO-GCaMP6s into the SON of Dbh^{flp+} x $Avp^{ires\text{-}Cre+}$ mice (Fig. 5j). We then measured AVP neuron population $[Ca^{2+}]_i$ activity (with *in vivo* fibre photometry) and plasma glucagon following inhibition of A1/C1 neurons with CNO (Fig. 5j and

Supplementary Fig. 8c). AVP neuron population activity during an ITT was reduced by A1/C1 silencing compared to vehicle injection (Fig. 5k-m). Furthermore, glucagon secretion was reduced following CNO silencing of A1/C1 neurons (Fig. 5n). Together, these data suggest that AVP-dependent glucagon secretion during an ITT is mediated by A1/C1 neurons.

AVP-induced glucagon secretion maintains glucose homeostasis during dehydration

Collectively, these data point to AVP being an important regulator of glucagon secretion but they do not explain why a receptor for a hormone commonly known for its anti-diuretic action is expressed in alpha-cells. We speculated that glucagon may play an important homeostatic role during dehydration - a physiological state where circulating AVP is elevated.

To explore this, mice were water restricted for 24 hours, but given unrestricted access to food. This resulted in a reduction in food intake (Fig. 6a) – a critically important behavioural response to water restriction known as dehydration anorexia (Watts & Boyle, 2010). Despite the 30% reduction in food intake, plasma glucose was maintained (Fig. 6b). We hypothesised that this was due to AVP-induced glucagon secretion. In support of this hypothesis, glucagon was indeed elevated in these animals following 24 hour water restriction (Fig. 6c). In contrast, when the same mice were given *ad lib* access to water (which would not elevate plasma AVP) but had their food consumption restricted to that consumed in the dehydration trial, blood glucose fell and plasma glucagon was not elevated (Fig. 6b, c). The elevation in plasma glucagon was due to AVP, because pre-treatment with the V1bR antagonist SSR149415 (or vehicle) during water deprivation, blunted this increase (Fig. 6d, e).

Therefore, in addition to serving an antidiuretic function, AVP stimulates glucagon secretion to aid the maintenance of plasma glucose in the dehydrated state (in spite of the reduction in feeding).

Insulin-induced AVP secretion may underlie counter-regulatory glucagon secretion in human, and is diminished in subjects with Type 1 Diabetes

To understand whether this physiological pathway contributes to counter-regulatory glucagon secretion in human, samples were analysed from an ongoing clinical trial (NCT03954873). In two "saline arms" of the trial, healthy volunteers were given a hypoglycaemic clamp during one visit and a euglycaemic clamp during another visit in a randomized order (Fig. 7a-d; see also Supplementary Fig. 9a-b). In response to hypoglycaemia (blood glucose of 2.8±0.1 mM, Fig. 7a), plasma glucagon rose (Fig. 7b) and so did plasma copeptin (Fig. 7c). In contrast, during euglycaemia (blood glucose of 5.1±0.1 mM), plasma glucagon (Fig. 7a) and copeptin (Fig. 7b) fell. There was a linear correlation between glucagon and copeptin in the samples taken from both eu- and hypoglycaemic clamps (Fig. 7d).

To understand whether circulating AVP could be contributing to counter-regulatory glucagon secretion in human subjects, islets isolated from human donors were studied. In human islets from 8 donors, *AVPR1B* was the most abundant of the vasopressin receptor family (Fig. 7e). These data are supported both by a recent meta-analysis of single-cell RNA-seq data from human donors (Mawla & Huising, 2019), and bulk sequencing of human islet fractions (Nica *et al.*, 2013). In human islets from 9 donors, AVP resulted in an increase in glucagon secretion (Fig. 7f). Finally, AVP increased Ca^{2+} (Fluo-4) activity in islets isolated from 5 human donors (Fig. 7g-h).

In T1D, deficiency of the secretory response of glucagon to hypoglycaemia is an early (< 2 years of onset) acquired abnormality of counter-regulation and leads to severe hypoglycaemia (Cryer, 2002). We therefore measured copeptin and glucagon during hypoglycaemic clamps in subjects with T1D and healthy controls from two previously published studies conducted on male participants (Christensen *et al.*, 2011; Christensen *et al.*, 2015). The BMI and age of these subjects did not differ (Supplementary Table 1). At 60 minutes, the achieved glucose clamp was similar between the subjects (Fig. 8a; see also Supplementary Fig. 9c-d). However, copeptin was significantly elevated in controls but not subjects with T1D (Fig. 8b). Insulin-induced hypoglycaemia failed to increase circulating glucagon in all subjects with T1D (Fig. 8d). Finally, a correlation of copeptin and glucagon demonstrated that control subjects either had a greater change in copeptin in response to hypoglycaemia, or a similar change in copeptin but this resulted in a larger increase in plasma glucagon (Fig. 8d).

Discussion

In this study, we report that AVP is an important regulator of glucagon secretion *in vivo*. This axis between the pituitary and the alpha-cell appears to be important for maintaining plasma glucose during dehydration as well as mediating the classical counter-regulatory response to hypoglycaemia. It would therefore appear that AVP regulates multiple physiological parameters that facilitate survival during stress, including water retention, blood pressure and plasma glucose.

Is AVP mediating glucagon secretion during counter-regulation?

The ability of exogenous AVP and AVP analogues to potently stimulate glucagon secretion *ex vivo* and *in situ* has been known for some time (Dunning *et al.*, 1984). However, the physiological role of AVP *in vivo* in regulating glucagon secretion has remained enigmatic because previous studies have employed *in vitro* or *in situ* methods (Dunning *et al.*, 1984; Gao *et al.*, 1990; Gao *et al.*, 1992; Li *et al.*, 1992; Yibchok-Anun *et al.*, 2000). Furthermore, these studies have used supraphysiological concentrations of AVP (Gao *et al.*, 1990), immortalised islet cell lines (Yibchok-Anun *et al.*, 2000) and/or synthetic AVP analogues (Dunning *et al.*, 1984).

Importantly, our data demonstrate that glucagon is controlled by systemic concentrations of AVP *in vivo* under various physiological and non-physiological challenges. Therefore, we suggest that the increase in *Avpr1b* expression in response to interrupted glucagon signalling (Kim *et al.*, 2017) is an exploitation of an important, established regulatory pathway from the hypothalamus to the islet alpha-cell (although we recognise that the phenotype in these mice is driven by hyperaminoacidaemia).

We did not observe an effect of AVP on insulin secretion from isolated mouse islets, whether at low or high glucose. In contrast, earlier studies have demonstrated that AVP stimulates insulin secretion (Dunning *et al.*, 1984; Gao *et al.*, 1990; Gao *et al.*, 1992; Li *et al.*, 1992). The physiological interpretation of these earlier studies is difficult because the V1bR is the only receptor from the vasopressin receptor family expressed in mouse islets, and its expression is restricted to alpha-cells (DiGruccio *et al.*, 2016; Taveau *et al.*, 2017), something we also observe. An explanation for the reported increase in insulin could lie in the recently elucidated role of glucagon as a paracrine regulator of insulin (Svendsen *et al.*, 2018). In particular, it could be that AVP stimulates glucagon secretion so potently (especially at the supraphysiological concentrations used in these aforementioned studies; > 10 nM) that it binds to the GLP-1 receptor on beta-cells, thereby increasing insulin secretion.

A1/C1 neurons mediate the AVP response to insulin-induced hypoglycaemia

Catecholaminergic neurons in the VLM are a key component of the central counter-regulatory circuit and the ability of these neurons to evoke hyperglycaemia (Ritter *et al.*, 2000; Zhao *et al.*, 2017; Li *et al.*, 2018) and hyperglucagonaemia (Andrew *et al.*, 2007) is well-established. Recent studies have clearly demonstrated that spinally-projecting C1 neurons evoke hyperglycaemia by stimulating the adrenal medulla (Zhao *et al.*, 2017; Li *et al.*, 2018), suggesting that the response is likely to be mediated by corticosterone and/or adrenaline. We also show that activation of A1/C1 neurons evokes hyperglycaemia, but by promoting glucagon release. The important distinction here is that the elevation of plasma glucagon cannot be explained by signalling from adrenal factors, because neither corticosterone nor adrenaline stimulated glucagon release or Ca^{2+} activity in isolated mouse and human islets when applied at circulating concentrations. Neurons in the VLM have a well-documented ability to increase plasma AVP (Ross *et al.*, 1984; Madden *et al.*, 2006).

Our data strongly support the notion that the hyperglycaemic and hyperglucagonaemic effect of activating A1/C1 neurons is, at least in part, mediated by stimulation of AVP release: we show that A1/C1 neurons send functional projections to the SON, A1/C1 function is required for insulin-induced AVP neuron activation and that AVP is an important stimuli of glucagon secretion. However, we recognise that other circuits must be involved in the activation of AVP neurons. For example, the PVN is richly supplied with axons from the BNST (Sawchenko & Swanson, 1983) and hypothalamic VMN neurons - key drivers of the glucose counter-regulatory response - project to the BNST (Meek *et al.*, 2016). Therefore a VHN-BNST circuit may also be important for driving AVP neuron activity in response to hypoglycaemia, explaining why A1/C1 inhibition only partially prevented the activation of AVP neurons. In addition, AVP can stimulate glycogen breakdown from the liver (Hems & Whitton, 1973). Therefore it is likely that part of the increase in plasma glucose following A1/C1 neuron stimulation is mediated by the action of AVP on the liver. While there may be direct effects of AVP on hepatic glucose production, the findings presented here demonstrate that inhibition of either AVP signalling or glucagon secretion during stimulation of A1/C1 neurons abolishes the increase in plasma glucose.

The signal driving AVP neuron activation is unlikely to be due to a direct action of insulin on AVP or A1/C1 neurons, because 2-DG caused a similar activation. The widely accepted view is that the activation of A1/C1 neurons (and consequently AVP neurons) during hypoglycaemia depends on peripheral glucose sensing at multiple sites, including the hepatic portal system (Marty *et al.*, 2007; Verberne *et al.*, 2014). The exact location of the glucose sensing is still controversial. Here, we show that activity of AVP neurons is increased at ~4.9 mM glucose; while it is unknown whether this threshold is sufficient to directly activate A1/C1 neurons, vagal afferents in the hepatic portal vein – which convey vagal sensory

information to the A1/C1 neurons via projections to the nucleus of the solitary tract (Verberne *et al.*, 2014) - are responsive to alterations in glucose at this threshold (Niijima, 1982). We therefore suggest that activation of A1/C1 neurons and the subsequent increase in AVP release is critical for counter-regulatory glucagon release during the early stages of hypoglycaemia (4-5 mM glucose), when intrinsic islet mechanisms are yet to be recruited.

Relevance of findings to diabetes and diabetes complications

The present findings may have clinical relevance. Insulin-induced hypoglycaemia is a major safety concern with diabetic patients (Cryer, 2002). Patients with type 1 diabetes acquire early abnormalities in their counter-regulatory response, putting them at increased risk of hypoglycaemia (McCrimmon & Sherwin, 2010). We found that hypoglycaemia fails to stimulate glucagon secretion in our cohort of T1D patients. This is a known, early acquired abnormality of counter-regulation in type 1 diabetes (Siafarikas *et al.*, 2012), which may in part be explained by the major structural and functional changes that occur to the islets in T1D. However, we also found that insulin-induced copeptin secretion was reduced, with some subjects exhibiting no elevation in copeptin. Therefore, part of this defective glucagon secretion may be due to an insufficient insulin-induced copeptin response. The cause for this change is unknown, but we speculate that recurrent hypoglycaemia in patients with T1D may result in changes in glucose and/or insulin sensitivity in the A1/C1 region. Regardless of the brain region involved in this attenuated copeptin response, monitoring of copeptin may prove an important tool for stratification of hypoglycaemia risk in patients with type 1 diabetes.

Back matter

Acknowledgements

We would like to thank the following for their invaluable input into this project: Prof. Yoichi Ueta, Dr. Stephen Lolait, Prof. Maurice Manning, Dr Craig Beall, Prof. Jeremy Tomlinson, Prof. Fredrik Karpe, Dr Aparna Pal, Dr Joachim Goedhart and Prof. David Hodson. We thank Dr. Claudia Guida, Dr. Reshma Ramracheya, Dr. Margarita Chibalina, Dr Belen Chanclon and Mr. Alex Früh for assistance with experiments and Dr. Andrei Tarasov for technical advice. We also thank Prof. W. Scott Young and Emily Shepard from NIMH for kindly providing us with *Avpr1b* knockout mice and Prof. Guy A. Rutter for hosting eye imaging experiments in his laboratory at Imperial College, UK.

We thank the Alberta Diabetes Institute IsletCore (University of Alberta, AB, Canada) for providing human islets, the isolation of which was supported in part by the Alberta Diabetes Foundation, the Human Organ Procurement and Exchange Program (Edmonton), and the Trillium Gift of Life Network (Toronto). We also thank Prof. Paul R.V. Johnson and colleagues at the Diabetes Research and Wellness Foundation Islet Isolation Facility. We would also like to thank the generosity of the organ donors and their families.

Funding

This study was funded by the following: Wellcome Senior Investigator Award (095531), Wellcome Strategic Award (884655), Sir Henry Wellcome Postdoctoral Fellowship (Wellcome, 201325/Z/16/Z), European Research Council (322620), Leona M. and Harry B. Helmsley Charitable Trust, Swedish Research Council, Swedish Diabetes Foundation, JRF from Trinity College, Goodger & Schorstein Scholarship (2017) and the Knut and Alice

Wallenberg's Stiftelse. J.G.K. and T.H. are supported by a Novo Nordisk postdoctoral fellowship run in partnership with the University of Oxford. J.A.K. holds a DPhil from the OXION Programme (Wellcome). P.E.M. holds a grant from the Canadian Institutes of Health Research (CIHR: 148451). B.B.L. is the recipient of grants from the NIH (R01 DK075632, R01 DK089044, R01 DK111401, R01 DK096010, P30 DK046200 and P30 DK057521). A.K. holds an NIH grant (F31 DK109575). V.S. is a Diabetes UK Harry Keen Clinical Fellow.

Data availability statement

The authors declare that all data supporting the findings of this study are available within the article and its Supplementary Information or from the lead author on reasonable request.

Author contributions

All authors collected and analysed the data. A.K and L.J.B.B. conceived the project and planned the experiments. L.J.B.B. wrote the initial draft of the manuscript. All authors edited and approved the subsequent drafts of the manuscript. V.S. and K.S. designed and performed the *in vivo* alpha cell imaging experiments. The clinical experiments in human participants were conducted by M.C. and T.M. in the lab of F.K.K.

Declaration of interests

The authors declare no competing interests.

Figure Legends

Figure 1: Insulin-induced hypoglycaemia enhances population activity of AVP neurons in the SON, driving glucagon secretion

a) Insulin tolerance test (ITT; 0.75 U/kg) in n=5 wild-type mice. Plasma glucose falls from ~8 mM to ~4 mM in 30 mins.

b) Plasma glucagon prior to, and 30 minutes following an ITT. n=5 wild-type mice. Paired t-test, p<0.01=**,

c) Glucagon secretion from isolated (*ex vivo*) mouse islets in response to different concentrations of glucose. n=7 wild-type mice. One-way ANOVA with Tukey post-hoc. 4 mM vs 8 mM glucose, p=0.99.

d) *In vivo* fibre photometry measurements of population GCaMP6s activity in pituitary-projecting AVP neurons in the supraoptic nucleus (SON). AAV-DIO-GCaMP6s was injected into the SON of *Avp*$^{ires\text{-}Cre+}$ mice. GCaMP6s was then imaged as indicated by the protocol in the horizontal bar.

e) Expression of GCaMP6s in AVP neurons in the SON. The tip of the optic fibre can be seen (arrow).

f) Raw population GCaMP6s activity (F) recording following an insulin tolerance test (ITT; 1.5 U/kg) and saline control. Baseline fluorescence (F_0) was calculated from signal 3 minutes prior to ITT/saline. Recordings contained an artefact from the injection (arrow) which was removed from plotted time-series and analysis.

g) *Upper panel:* heatmap of population activity (GCaMP6s) response to ITT for each mouse (n=6). Data represented as % of maximum signal. *Lower panel:* heatmap of population activity (GCaMP6s) response to saline vehicle for each mouse (n=6).

h) GCaMP6s signal (normalized) in response to insulin (n=6) or vehicle (n=6). GCaMP6s data represented as $(F\text{-}F_0)/F_0$.

i) Plasma copeptin at 30 minutes following either saline or insulin injection. Mann-Whitney U test, p=0.021. n=15 (saline) and n=18 (insulin).

Figure 2: Simultaneous continuous glucose monitoring (CGM) and *in vivo* fibre photometry of AVP neurons

a) Simultaneous continuous glucose monitoring (CGM) and *in vivo* fibre photometry of AVP neurons (in *Avp*$^{ires\text{-}Cre+}$ mice; as per Fig. 1d) in response to an ITT (1.0 U/kg; 3 trials; red) and saline (blue), in two mice. Dashed line indicates the time of injection (which is accompanied with an artefact in the GCaMP6 signal).

b) Zoom of each insulin trial from a). Dashed line indicates time of injection. In one trial, the glucose concentration at which the GCaMP6 signal first exhibited a peak (solid line), and first exceeded 2 SD (dashed-dot) and 3 SD (dot) of the baseline signal, are indicated. The 2-3 min period of baseline recording prior to the insulin injection is also depicted.

c) This analysis was conducted for each trial. Grouped analysis as depicted in b) of the glucose concentration at which the GCaMP6 signal crosses >2 SD from baseline, crosses > 3 SD from baseline and first exhibits a peak, following an insulin tolerance test. n=2 mice, 6 trials. One-way ANOVA, $p<0.05$=*.

d) Grouped analysis as depicted in b) of the delay (from insulin injection) taken for the GCaMP6 signal to cross >2 SD from baseline, cross > 3 SD from baseline and first exhibits a peak. n=2 mice, 6 trials. One-way ANOVA, $p<0.05$=*.

e) Body temperature following insulin injection (dashed line). Mean ± SEM of six trials in n=2 mice. Dotted line indicates (average) time GCaMP6 activity first exhibits a peak, as per d).

Figure 3: The vasopressin 1b receptor mediates insulin-induced glucagon secretion

a) Plasma glucagon following an ITT (0.5 U/kg; injection at 30 min). 30 min prior to the ITT (at 0 min), either the V1bR antagonist SSR149415 (30 mg/kg) or vehicle was administered i.p. Two-way RM ANOVA with Sidak's (between conditions) and Tukey's (within condition) multiple comparisons test. Vehicle vs. SSR149415; $p<0.01$=†† (60 minutes) and $p=0.08$ (90 minutes). Within the condition, SSR149415 did not increase glucagon secretion (all $p>0.6$ for 30 vs 60 and 90 min), whereas glucagon was increased in the vehicle treatment group (all $p<0.02$ for 30 vs 60 and 90 min). Time, $p<0.0001$; Treatment, $p=0.045$; Interaction, $p=0.016$. n=9 wild-type mice.

b) Blood glucose for cohort in (a). Two-way RM ANOVA. Time, $p<0.0001$; Treatment, $p=0.40$; Interaction, $p=0.51$. n=9 wild-type mice.

c) Same as a) but for a larger dose of insulin (0.75 U/kg).

d) Same as b) but for a larger dose of insulin (0.75 U/kg).

e) Plasma glucagon following an ITT (injection at 0 min) in *Avpr1b*$^{-/-}$ mice and littermate controls (*Avpr1b*$^{+/+}$). Two-way RM ANOVA with Sidak's multiple comparisons test. *Avpr1b*$^{-/-}$ vs. *Avpr1b*$^{+/+}$; $p<0.001$=††† (30 minutes). 0 vs. 30 minutes; $p<0.001$ (*Avpr1b*$^{+/+}$); $p=0.097$ (*Avpr1b*$^{-/-}$). Time, $p<0.0001$; Genotype, $p=0.008$; Interaction, $p=0.009$. n=8-9 mice. Note that even after removal of the two high plasma glucagon samples at 30 minutes in *Avpr1b*$^{+/+}$ mice, the glucagon is still higher than in *Avpr1b*$^{-/-}$ mice ($p=0.0028$).

f) Blood glucose for cohort in (c). Two-way RM ANOVA. Time, $p<0.0001$; Treatment, $p=0.40$; Interaction, $p=0.51$. n=8-9 mice.

g) Same as e) but for a larger dose of insulin (0.75 U/kg).

h) Same as f) but for a larger dose of insulin (0.75 U/kg).

i)

Figure 4: Metabolic response to elevating AVP *in vivo*

a) AAV-DIO-hM3Dq-mCherry was injected bilaterally into the supraoptic nucleus (SON) of *Avp*$^{ires\text{-}Cre+}$ mice. Mice were fasted for 4 hours (beginning at 10:00 am), and then CNO (or saline vehicle) was injected (3 mg/kg i.p.). In the same cohort, during a different trial, the glucagon receptor antagonist LY2409021 (5 mg/kg) or V1bR antagonist SSR149415 (30 mg/kg) was injected i.p. 30 minutes prior to CNO. The lower panel gives an overview of the protocol. Plasma glucose and glucagon were then measured. See also Supplementary Fig. 3.

b) Change in blood glucose from 0 min sample. Two-way RM ANOVA with Tukey's multiple comparison test. CNO 0 mins vs. CNO at 15, 30 and 60 mins; $p<0.05$=*, $p<0.01$=**. 30 mins comparison of CNO vs. Saline, CNO + LY2409021 or CNO + SSR149415 at 30 mins; $p<0.01$=††. Time, $p<0.0001$; Treatment, $p=0.0006$; Interaction, $p<0.0001$. N=6 mice.

c) As in (b), but plasma copeptin 30 minutes following saline (-) or CNO (+). N=12 mice. Mann Whitney t-test ($p=0.0025$). N=18 mice. Removal of < 1 pg/ml measurements (N=3 in saline treatment) yields $p=0.007$.

d) As in (b), but plasma glucagon at 30 mins following saline (-) or CNO (+) injection. Represented as % of baseline glucagon (0 min). N=11 mice. Mann-Whitney U test, $p=0.03$=*.

e) Islets from *Gcg*$^{Cre+}$-GCaMP3 mice were injected into the anterior chamber of the eye (ACE) of recipient mice (n=5 islets in 5 mice). After >4 weeks, GCaMP3 was imaged *in vivo* in response to i.v. AVP (10 µg/kg) or saline administration. Saline did not

change the GCaMP3 signal in all mice tested. AVP evoked an increase in calcium activity, typically starting with a large transient.

f) Response of alpha-cell to i.v. AVP. Lower panel shows raster plot of response in different cells.

g) Integrated F/F_0 (area under curve) response for all alpha-cells in recorded islets (5 islets, N=3 mice). The area under the curve was calculated 30 secs before i.v. injection, 30 secs after and 120 secs after. One-way RM ANOVA with Tukey's multiple comparison test; $p<0.01$=**.

h) Image of islets (arrows) engrafted in the ACE.

Figure 5: Insulin-induced AVP secretion is mediated by A1/C1 neurons

a) *Upper panel:* AAV-DIO-ChR2-mCherry was injected into the VLM of Th^{Cre+} mice or Avp^{GFP} x Th^{Cre+} mice, targeting A1/C1 neurons. Brains were then prepared for viral projection mapping or channelrhodopsin2-assisted circuit mapping (CRACM), respectively. *Lower panel:* CRACM. Excitatory post-synaptic currents (EPSCs) were recorded in voltage-clamp mode in GFP^+ (AVP) and GFP^- neurons in the SON and PVH. The number (n) of neurons that responded to opto-activating A1/C1 terminals. Total of 36 neurons recorded. See also Supplementary Fig. 7a.

b) *Upper panel:* Viral expression of ChR2-mCherry in A1/C1 neurons. *Lower panel:* A1/C1 neuron terminals co-localise with AVP-immunoreactive neurons.

c) *Left panel:* EPSCs evoked by opto-activation of A1/C1 terminals with 473 nm light pulses (arrows). *Right panel:* Light-evoked EPSCs following application of DNQX (20 µM).

d) EPSC waveforms in a single GFP^{+} (AVP) neuron in response to repeated opto-activation of A1/C1 neuron terminals. Mean and SD of all EPSCs shown in black line and shaded area. Timing of light pulse shown in blue bar.

e) EPSCs evoked by opto-activating A1/C1 terminals at baseline (*left*) and following addition of TTX (1 µM*; middle*) and 4-AP (1 mM*; right*).

f) AAV-DIO-hM3Dq was injected into Th^{Cre+} mice, targeting A1/C1 neurons. CNO (1 mg/kg) was then injected (i.p.). Antagonists (or vehicle) for the V1bR (SSR149415, 30 mg/kg) or glucagon receptor (GCGR; LY2409021, 5 mg/kg) were injected 30 minutes prior to CNO. Plasma glucose and glucagon was then measured. See also Supplementary Fig. 7b,c.

g) Plasma glucose in response to CNO and pre-treatment with antagonists. N=8 mice. Two-way RM ANOVA (Sidak's multiple comparison's test).. Time ($p<0.0001$), Treatment ($p=0.03$) and Interaction ($p=0.0002$).

h) Same as (g), but 30 minute data only.

i) Plasma glucagon at 30 minutes post CNO (or vehicle) injection. Two-way RM ANOVA with Tukey's (within treatment) and Sidak's (between treatments) multiple comparisons. $p<0.05$=*, ns=not significant. Within treatment, CNO increased glucagon at 30 min vs. 0 min ($p=0.022$). Saline did not ($p=0.96$). Between treatments, CNO increased glucagon at 30 min vs. saline ($p=0.001$). N=6 mice. All data are represented as mean ± SEM.

j) *In vivo* fiber photometry measurements of population GCaMP6 activity in pituitary-projecting SON AVP neurons during A1/C1 neuron inhibition. AAV-DIO-GCaMP6s was injected into the SON and AAV-fDIO-hM4Di-mCherry into the VLM of $Avp^{ires\text{-}Cre+}$ x Dbh^{flp+} mice. GCaMP6s was then imaged in response to an insulin tolerance test

(ITT), following inhibition of the A1/C1 neuron (with CNO at 1 mg/kg), as indicated by the protocol in the lower horizontal bar. See Supplementary Fig. 8b.

k) Example population activity in one mouse in response to an ITT, following saline or CNO treatment (on different trials). Baseline fluorescence (F_0) was calculated from signal 3 minutes prior to ITT, and subtracted from the fluorescence signal (F).

l) *Left panel:* Average GCaMP6 signal (normalized) in response to insulin with saline pre-treatment (N=9 mice). *Right panel:* Average GCaMP6 signal in response to insulin with CNO pre-treatment (N=9). GCaMP6 signal is normalized to baseline ($(F-F_0)/F_0$).

m) Binned population activity (normalized GCaMP6 signal) following an ITT with pretreatment of CNO or saline. One-way RM ANOVA; CNO *vs.* Saline, $p<0.001$=†††. N=9 mice in each treatment. Bin width = 3 minutes.

n) Plasma glucagon in response to an ITT, following CNO (or saline) injection (to inhibit A1/C1 neurons). Two-way RM ANOVA by both factors with Bonferroni's multiple comparisons test. Saline vs. CNO; $p<0.05$=* (30 mins); $p>0.99$ (0 mins). 0 vs. 30 mins; p=0.005 (Vehicle); p=0.0293 (SSR149415). Time, p=0.028; Treatment, p=0.032; Interaction, p=0.027. N=6 wild-type mice.

Figure 6: AVP-induced glucagon secretion during dehydration

a) AVP-induced glucagon secretion during dehydration. Wild-type mice were first subjected to a 24 hour water restriction trial, wherein food consumption during was monitored. During the second trial (food restriction trial), the same mice were given unrestricted access to water, but had the same quantity of food available consumed in the first (water restriction) trial. One-way RM ANOVA; Dunnett's post-hoc, $p<0.05$=*. N=8 wild-type mice.

b) Blood glucose in the water and food restriction trial. Two way RM ANOVA by both factors; $p<0.05$=* and ns=0.71 (within trial); $p<0.01$=†† (between trials). Tukey's multiple comparison tests. N=8 wild-type mice.

c) *Left panel:* Plasma glucagon in the water and food restriction trial. Two way RM ANOVA by both factors; $p<0.05$=** and ns=0.49 (within trial). Tukey's multiple comparison tests. *Right panel:* Same data, represented as plasma glucagon at 24 hour minus 0 hours. Mann Whitney-U paired t-test (p=0.023). N=8 wild-type mice.

d) *Left panel:* Plasma glucagon before and after 24 hour water restriction, where either vehicle or the V1b receptor antagonist SSR149415 (30 mg/kg) was injected 90 minutes prior to termination of the restriction. Two way RM ANOVA by both factors; $p<0.01$=**, ns=not significant. Tukey's multiple comparison tests. *Right panel:* Same data, represented as plasma glucagon at 24 hour minus 0 hours. Mann Whitney-U paired t-test ($p<0.01$=**). N=11-12 wild-type mice.

Figure 7: Insulin-induced hypoglycaemia evokes copeptin and glucagon secretion in human subjects

a) Blood glucose was clamped at euglycaemia (Eug) and followed during insulin-induced hypoglycaemia (Hypo). N=10 healthy human subjects. The data is from an ongoing clinical trial (NCT03954873). The clamp was initiated at time 0 min and terminated at 60 min.

b) Plasma copeptin measurement during and following clamping period. Represented as change in copeptin from baseline (time = 0 min). Two-way RM ANOVA by both factors. Indicated time point *vs.* 0 min; $p<0.05$=*, $p<0.01$=**. Between treatments; $p<0.05$=†. Raw data is shown in Supplementary Figure 9a.

c) Plasma glucagon measurement during insulin-induced hypoglycaemia. Two-way RM ANOVA by both factors. Time point *vs.* 0 min; $p<0.05$=*. Between treatments; $p<0.05$=†. Represented as change in glucagon from 0 min time point. Raw data is shown in Supplementary Figure 9b.

d) Correlation of change in copeptin and change in glucagon, with a linear regression (dashed line).

e) mRNA expression of *AVPR1A*, *AVPR1B*, AVPR2 and *OXTR* in human islets. Human islet samples N=7-8 donors. Calculated with the Pfaffl method, using *Actb* as the reference gene.

f) Glucagon secretion from islets isolated from human donors, in response to AVP. One-way ANOVA, $p<0.05$=*. N=5-9 human donors.

g) Fluo4 signal from a putative alpha-cell in a human islet in response to AVP (10, 100 and 1000 pM). Recording in 3 mM glucose.

h) Area under curve (AUC, normalized to duration) for Fluo4 signal in each human islet, for each experimental condition. 26 islets, N=4 human donors. One-way ANOVA, $p<0.05$=*; $p<0.001$=***.

Figure 8: Insulin-induced copeptin and glucagon secretion is diminished in type 1 diabetic subjects

i) Hypoglycaemia was induced by an insulin infusion in patients with T1D (N=10; Christensen *et al.* (2015)) and non-diabetic individuals (Controls; N=10; Christensen *et al.* (2011)). The insulin infusion was initiated at 0 min and terminated at 90 min. See Supplementary Table 1 for details of these two cohorts.

j) Plasma copeptin measurement during and following clamping period. Represented as change in copeptin from baseline (time = 0 min). Two-way RM ANOVA by both

factors. Time point *vs.* 0 min; $p<0.05$=*, $p<0.01$=**. Between groups; $p<0.05$=†. Raw data is shown in Supplementary Figure 9c.

k) Plasma glucagon measurement during the clamping period. Two-way RM ANOVA by both factors. Time *vs.* 0 min; $p<0.05$=*. Between groups; $p<0.05$=†. Represented as change in glucagon from 0 min time point. Raw data is shown in Supplementary Figure 9d.

l) Correlation of change in copeptin and change in glucagon following hypoglycaemic clamping for control subjects (circle) and T1D (square).

Supplementary Figure Legends

Supplementary Figure 1: alpha-cell output is not increased by systemic concentrations of cortisol or adrenaline

a) Glucagon secretion from mouse islets in response to varying concentrations of adrenaline (Adr). One-way ANOVA; p<0.05=*, p<0.001=***. N=11 wild-type mice,

b) Same as in a) but for islets from N=6 human donors. All static incubations in triplicates (1 mM glucose). One-way ANOVA; ns=not significant (p>0.96).

c) *Upper panel:* GCaMP3 signal from an alpha-cell in response to various Adr concentrations. Confocal recording from an intact islet isolated from a *Gcg*$^{Cre+}$-GCaMP3 mouse. *Lower panel:* frequency of GCaMP3 oscillations in response to various Adr concentrations. 85-90 alpha-cells, 6 islets, N=5 *Gcg*-GCaMP3 mice. One-way ANOVA, ns=not significant (p>0.99).

d) Glucagon secretion from mouse islets in response to varying concentrations of corticosterone. N=6 wild-type mice. One-way ANOVA; p<0.05=*, p<0.001=***, ns=not significant (p>0.96).

e) Same as in (c) but for corticosterone. 152-157 alpha-cells, 6 islets, N=5 *Gcg*$^{Cre+}$-GCaMP3 mice. One-way ANOVA, ns=not significant (p>0.99).

All data are represented as mean ± SEM.

Supplementary Figure 2: AVP mediates hyperglycaemia and hyperglucagonaemia in response to 2DG

a) *In vivo* fibre photometry measurements of population GCaMP6s activity in pituitary-projecting AVP neurons in the supraoptic nucleus (SON). GCaMP6s was imaged in

response to 2-Deoxy-D-glucose (2DG, 500 mg/kg) injection (i.p.). Plasma glucose at baseline (0 min) and 30 min after 2DG injection. Paired t-test, $p<0.01$=**. N=6 mice.

b) Example recording of population GCaMP6s activity in one mouse after 2DG injection.

c) *Upper panel:* heatmap of population activity (GCaMP6s) response to 2DG for each mouse (N=6). *Lower panel:* mean ± SEM GCaMP6s signal for all mice (N=6) in response to 2DG. GCaMP6s data represented as $(F-F_0)/F_0$.

d) Binned population activity (normalized GCaMP6 signal) following 2DG. One-way RM ANOVA. N=6 mice in each treatment. Bin width = 3 minutes.

e) *Left panel:* Blood glucose in response to 2DG with or without pre-treatment with the V1bR (SSR149415, 30 mg/kg) or glucagon receptor (LY2409021, 5 mg/kg) antagonists. Antagonists (or vehicle) for were injected 30 minutes prior to 2DG. Blood glucose was then measured. Data represented as change in blood glucose prior to 2DG injection. Two-way RM ANOVA with Sidak's multiple comparison test; 2DG vs. 2DG + SSR149415 and 2DG + LY024091, $p<0.05$=*. Main effect: 2DG vs. 2DG + SSR149415, p=0.023; 2DG vs. 2DG + LY2409021, p=0.0169. N=8 wild-type mice. *Right panel:* Glucose area under the curve (AUC) in response to 2DG. One way RM ANOVA with Dunnett's multiple comparison test. $p<0.05$=*. N=8 wild-type mice of both sex.

f) Plasma glucagon following 2DG injection (injection at 0 min); distinct cohort to m). Prior to the 2DG, either the V1bR antagonist SSR149415 or vehicle was administered i.p. Two-way RM ANOVA by both factors with Bonferroni's multiple comparisons test. Vehicle vs. SSR149415; $p<0.01$=†† (30 mins); $p>0.99$ (0 mins). 0 vs. 30 mins; p=0.009 (Vehicle); p=0.093 (SSR149415). Time, $p<0.0001$; Treatment, p=0.002; Interaction, p=0.005. N=6 male wild-type mice.

Supplementary Figure 3: Effects of CNO in animals expressing mCherry in SON AVP neurons

a) AAV-DIO-hM3Dq-mCherry was injected into the supraoptic nucleus (SON) of *Avp*$^{ires\text{-}Cre+}$ mice. Patch-clamp recording from mCherry^{+} neuron in the SON in response to CNO. Firing frequency was increased in response to CNO. See Fig. 1.

b) Grouped data for firing frequency response to CNO in 3 mCherry^{+} neurons from SON of N=2 mice, as described in a). One-way ANOVA; before treatment (-) vs CNO, p=0.11. CNO concentration applied was 5-10 µM. See Fig. 1.

c) Immunostaining for AVP in the SON of an *Avp*$^{ires\text{-}Cre+}$ mouse with AAV-DIO-hM3Dq-mCherry injected into the SON, as described in a).

d) Staining for mCherry; same brain sample as c).

e) Merge of c) and d).

f) Food intake in response to CNO in *Avp*$^{ires\text{-}Cre+}$ mice expressing hM3Dq in the SON. Two-way RM (both factors) ANOVA (Time, $p<0.001$; Treatment, $p=0.52$). N=11 mice.

g) AAV-DIO-mCherry was injected into the supraoptic nucleus (SON) of *Avp*$^{ires\text{-}Cre+}$ mice, yielding mCherry expression in AVP neurons. CNO (3 mg/kg; i.p.) was injected and blood glucose measured (control experiments for Fig. 1b). One-way RM ANOVA (Time, $p=0.26$). N=7 mice. For comparison, the saline injections from Fig. 1b are also shown, wherein saline was injected i.p. into mice expressing hM3Dq in AVP neurons in the SON.

h) Response of blood glucose to exogenous AVP (5 µg/kg) during continuous glucose monitoring. Representative of 6 trials from N=2 mice.

i) AVP (10 µg/kg, i.p.) was injected into wild-type mice and blood glucose was measured with glucose test strips. Two-way RM ANOVA with Tukey's (within treatments) and Sidak's (between treatments) multiple comparison. AVP injection caused an increase in plasma glucose at 15 min compared to 0 min ($p=0.023$, *). Vehicle did not increase plasma glucose (all $p>0.2$). At 15 mins, blood glucose for AVP treatment was significantly different to saline treatment ($p=0.038$, †).

j) Same cohort as in (e), but plasma glucagon measurements. Two-way RM ANOVA; $p<0.05$=*.

Supplementary Figure 4: Expression of the vasopressin 1b receptor in mouse

a) mRNA expression of *Avpr* family in mouse heart, kidney, islets and adrenal glands. Samples from N=3 wild-type mice, each run in triplicate. Calculated with the Pfaffl method, using *Actb* as the reference gene.

b) mRNA expression in sorted islet cells. Fractions were sorted from mice with a fluorescent reporter (RFP) in alpha-cells (*Gcg*$^{Cre+}$-RFP mice) into an alpha-cell fraction (RFP(+)) and non-alpha-cell fraction (RFP(-)). Data from 4 sorts from N=4 *Gcg*$^{Cre+}$-RFP mice. Ratio paired t-test; $p<0.05$=*, $p<0.01$=**.

c) Same data as in c). mRNA expression in alpha-cells (RFP(+) fraction) represented as fold of RFP(-) expression. Scale = $\log_{10}$. All data represented as mean ± SEM.

Supplementary Figure 5: AVP increases glucagon secretion *ex vivo* and *in situ*

a) Glucagon secretion from isolated mouse islets in response to AVP. One-way ANOVA ($p<0.05$=*; $p<0.01$=**; $p<0.001$=***). N=12 wild-type mice.

b) Insulin secretion from isolated mouse islets in response to physiological (10-100 pM) and supra-physiological (100 nM) concentrations of AVP. One-way ANOVA, $p<0.01$=**. N=5 wild-type mice.

c) Glucagon secretion from isolated mouse islets in response to AVP in the presence and absence of the V1bR antagonist SSR149415. One-way ANOVA ($p<0.05$=*; $p<0.01$=**). N=7 wild-type mice.

d) Glucagon secretion from the perfused mouse pancreas in response AVP (10 nM). All data are represented as mean ± SEM. N=5 mice.

e) Glucagon secretion (pM) from isolated mouse islets in response to AVP. One-way ANOVA ($p<0.05$=*). N=5-6 wild-type mice. AVP was applied in high (15 mM glucose).

f) Glucagon secretion (% content) from isolated mouse islets in response to AVP. One-way ANOVA ($p<0.05$=*). N=5-6 wild-type mice. AVP was applied in high (15 mM glucose).

g) Insulin secretion (mU/L) from isolated mouse islets in response to AVP. One-way ANOVA, $p<0.01$=**. N=5 wild-type mice. AVP was applied in high (15 mM glucose).

h) Insulin secretion (% content) from isolated mouse islets in response to AVP. One-way ANOVA, $p<0.01$=**. N=5 wild-type mice. AVP was applied in high (15 mM glucose).

i) Membrane potential (V_M) recording (perforated patch-clamp) of an alpha-cell in response to 100 pM AVP. Recording in 3 mM glucose. All recordings from intact islets isolated from *Gcg*-GCaMP3 mice.

j) Frequency-response curve for varying concentrations of AVP (17 alpha-cells, 10 *Gcg*-GCaMP3 mice). Mixed-effects analysis of variance, Holm-Sidak's post-hoc ($p<0.01$=**, $p<0.001$=*** and $p=0.073$ for 3 mM glucose vs. 10 pM AVP).

k) *Upper panel:* GCaMP3 signal from an alpha-cell in response to varying AVP concentrations. *Lower panel:* binned Ca^{2+} (GCaMP3) events from an intact islet (58 cells) in response to an AVP dose-response curve (concentrations in pM). Bin width = 7.8 seconds.

l) Box and whisker plot of the frequency of GCaMP3 oscillations in response to AVP. 142-170 alpha-cells, 7 islets, N=7 *Gcg*-GCaMP3 mice. Recordings in 3 mM glucose. One-way RM ANOVA, $p<0.001$=***.

m) GCaMP3 signal from an alpha-cell in response to 100 pM AVP in the presence and absence of the V1bR antagonist SSR149415 (10 µM). *Lower panel:* binned Ca^{2+} (GCaMP3) events from all alpha-cells (16 cells) in the same recording.

n) Frequency of GCaMP3 oscillations in response to 100 pM AVP in the presence and absence of SSR149415 (10 µM). 75-90 alpha-cells, 6 islets, N=5 *Gcg*-GCaMP3 mice. Recordings in 3 mM glucose. One-way ANOVA, $p<0.001$=***, ns=not significant ($p=0.513$).

Supplementary Figure 6: AVP evokes glucagon secretion via the canonical Gq pathway.

a) GCaMP3 signal from an alpha-cell from a Gcg^{Cre+}-GCaMP3 mouse in response to 100 pM AVP in the presence and absence of the G_q inhibitor YM-254890 (0.2 µM). *Lower panel:* binned Ca^{2+} (GCaMP3) events from all alpha-cells (20 cells) in the same recording.

b) Frequency of GCaMP3 oscillations in response to 100 pM AVP in the presence and absence of the V1b receptor antagonist SSR149415 (10 µM). 75-90 alpha-cells, 6 islets, N=5 *Gcg*$^{Cre+}$-GCaMP3 mice. Recordings in 3 mM glucose. One-way ANOVA, p<0.001=***, ns=not significant (p=0.513).

c) Heatmap of intracellular diacylglycerol (DAG; Upward DAG) signal from single islet cells (dispersed into clusters) in response to AVP. The signal was median filtered and normalized to largest signal in the recording.

d) Area under curve (AUC, normalized to duration) for DAG signal for each experimental condition. 10 recordings, 152 cells, N=3 wild-type mice. One-way ANOVA, p<0.001=***, ns=not significant (p=0.513).

e) *Upper panel:* V_M (moving-average filtered) in 3 mM glucose with or without AVP. *Lower panel:* Power spectrum analysis of moving-average filtered V_M in 3 mM glucose alone and with 10 pM AVP. Power spectrum normalized to total power.

f) Schematic of mathematical model of IP3-induced Ca^{2+} oscillations. AVP binds to the V1bR and activates the associated G-protein (G). The G-protein drives hydrolysis of PIP2 which cleaves to form IP3. IP3 can then activate IP3R on the membrane of the ER, increase the efflux of Ca^{2+} from the ER into the cytoplasm (J_{IP3R}). Ca^{2+} contributing to cytoplasmic Ca^{2+} concentration: J_{serca} (SERCA pump), J_{leak} (leak Ca^{2+} flux) and (flux due to IP3R activation). IP3 either degrades (at rate k_{deg}) or activates IP3R. ER = endoplasmic reticulum.

g) Simulated Ca^{2+} oscillations in response to a step increase in receptor ligand (AVP). See supplementary information for equations and parameters of model.

Supplementary Figure 7: Viral tracing of A1/C1 terminals

a) Injection of a Cre-dependent viral vector containing the light-gated ion channel Channelrhodopsin-2 (AAV-DIO-ChR2-mCherry) into A1/C1 neurons of *Th*$^{Cre+}$ mice. *Top left:* mCherry expression in A1/C1 neurons (white box). *Top right:* mCherry expression in the PVH and SON. *Bottom left:* AVP-immunoreactive neurons (green) expression in the PVH and SON. *Bottom right:* A1/C1 terminals (mCherry) co-localizing with AVP neurons (green) in the PVH and SON.

b) Expression of hM3Dq in A1/C1 neurons, following AAV-DIO-hM3Dq-mCherry injection into the A1/C1 region of *Th*$^{Cre+}$ mice (i). TH = tyrosine hydroxylase.

c) CNO administration (i.p.) into *Th*$^{Cre+}$ mice expressing mCherry (and not hM3Dq) in A1/C1 neurons (control experiments for Fig. 5f-i). The saline injections in mice expressing hM3Dq in A1/C1 neurons (from Fig. 5f-i) are also shown for comparison.

Supplementary Figure 8: c-fos expression in A1/C1 neurons during an ITT

a) *Left: c-fos* expression 30 minutes following i.p. saline injection. *Right:* Same animal, but merge of *Th* and *c-fos*. Note the *Th*$^{+}$ immunoreactive neurons in the A1/C1 region (white box).

b) *Left: c-fos* expression in *Th*$^{Cre+}$ mice following an 30 minutes following i.p. insulin injection. *Right:* Same animal, but merge of *Th* and *c-fos*. Note the *Th*$^{+}$ immunoreactive neurons in the A1/C1 region (white box) co-expressing *c-fos*. *Lower panel:* Magnified view of *c-fos* and *Th* in A1/C1 neurons 30 minutes following insulin injection. Images representative of experiments in N=1+1 mice. See Fig. 5.

c) *Top left:* Expression of mCherry and TH (green) in A1/C1 neurons (white box) of *Dbh*$^{flp+}$ mice, following viral injection of AAV-fDIO-hM4Di-mCherry into the VLM, targeting A1/C1 neurons. *Top right:* Magnified view of the A1/C1 region, TH

expression. *Bottom left:* Magnified view, mCherry expression. *Bottom right:* merge. TH = tyrosine hydroxylase.

Supplementary Figure 9: Raw glucagon and copeptin data from human studies

a) Raw copeptin values from Fig. 7b. Two-way RM ANOVA by both factors. Indicated time point *vs.* 0 min; $p<0.05$=*. Between treatments; $p<0.05$=†.

b) Raw glucagon values from Fig. 7c. Two-way RM ANOVA by both factors. Indicated time point *vs.* 0 min; $p<0.01$=**, ns=not significant. Between treatments; $p<0.05$=†, ns=not significant.

c) Raw copeptin values from Fig. 8b. Two-way RM ANOVA by both factors. Indicated time point *vs.* 0 min; $p<0.05$=*, ns=not significant. Between groups; $p<0.05$=†, ns=not significant.

d) Raw glucagon values from Fig. 8c. Two-way RM ANOVA by both factors. Indicated time point *vs.* 0 min; $p<0.01$=*. Between groups; $p<0.05$.

Supplementary Table 1: Participant characteristics for Fig. 8

	Christensen *et al.* (2011)	Christensen *et al.* (2015)	p
Cohort	Control (N=10)	T1D (N=10)	
Age (years)	23±1	26±1	0.055
BMI (kg/m^2)	23±0.5	24±0.5	0.1744
HbA1c (%)	5.5±0.1	7.3±0.2	<0.0001

Methods

Ethics

All animal experiments were conducted in strict accordance to regulations enforced by the research institution. Experiments conducted in the UK were done so in accordance with the UK Animals Scientific Procedures Act (1986) and University of Oxford and Imperial College London ethical guidelines, and were approved by the local Ethical Committee. All animal care and experimental procedures conducted in the U.S.A. were approved by the Beth Israel Deaconess Medical Center Institutional Animal Care and Use Committee. Animal experiments conducted in Goteborg University were approved by a local Ethics Committee.

Human pancreatic islets were isolated, with ethical approval and clinical consent, at the Diabetes Research and Wellness Foundation Human Islet Isolation Facility (OCDEM, Oxford, UK) or Alberta Diabetes Institute IsletCore (University of Alberta, AB, Canada). Islets from a total of 19 human donors were used in this study. Donor details were as follows; age = 42 ± 4 years; BMI = 27.1 ± 3; Sex = 10/9 (M/F).

Animals

All animals were kept in a specific pathogen-free (SPF) facility under a 12:12 hour light:dark cycle at 22 °C, with unrestricted access to standard rodent chow and water. C57BL/6J mice used in this study are referred to as wild-type mice. To generate alpha-cell specific expression of the genetically-encoded Ca^{2+} sensor GCaMP3, mice carrying Cre recombinase under the control of the proglucagon promoter (Gcg^{Cre+} mice) were crossed with mice with a floxed green calmodulin (GCaMP3) Ca^{2+} indicator in the ROSA26 locus (The Jackson Laboratory). These mice are referred to as *Gcg*-GCaMP3 mice. To generate mice expressing RFP in alpha-cells, Gcg^{Cre+} were crossed with mice containing a floxed tandem-dimer red fluorescent

protein (tdFRP) in the ROSA26 locus (*Gcg*-RFP mice). Both of these mouse models were kept on a C57BL/6J background. Other transgenic mouse strains used – namely, $Avp^{ires\text{-}Cre+}$ (Pei *et al.*, 2014), Th^{Cre+} (The Jackson Laboratory), Dbh^{flp+} (MMRCC) and Avp^{GFP} (MMRCC) - were heterozygous for the transgene and maintained on a mixed background. $Avpr1b^{-/-}$ and littermate controls ($Avpr1b^{+/+}$) were bred and maintained as previously described (Wersinger *et al.*, 2002).

Isolation of mouse islets

Mice of both sex and 11-16 weeks of age were killed by cervical dislocation (UK Schedule 1 procedure). Pancreatic islets were isolated by liberase digestion followed by manual picking. Islets were used acutely and were, pending the experiments, maintained in tissue culture for <36 hour in RPMI 1640 (11879-020, Gibco, Thermo Fisher Scientific) containing 1% pennicillin/streptomycin (1214-122, Gibco, Thermo Fisher Scientific), 10%FBS (F7524-500G, Sigma-Aldrich) and 11 mM glucose, prior to experiments.

Patch-clamp electrophysiology in islets

Mouse islets were used for patch-clamp electrophysiological recordings. These recordings (in intact islets) were performed at 33-34 ^{0}C using an EPC-10 patch-clamp amplifier and PatchMaster software (HEKA Electronics, Lambrecht/Pfalz, Germany). Unless otherwise stated, recordings were made in 3 mM glucose, to mimic hypoglycaemic conditions in mice. Currents were filtered at 2.9 kHz and digitized at > 10 kHz. A new islet was used for each recording. Membrane potential (V_M) recordings were conducted using the perforated patch-clamp technique, as previously described (Briant *et al.*, 2018). The pipette solution contained (in mM) 76 K_2SO_4, 10 NaCl, 10 KCl, 1 $MgCl_2 \cdot 6H_20$ and 5 Hepes (pH 7.35 with KOH). For these experiments, the bath solution contained (mM) 140 NaCl, 3.6 KCl, 10 Hepes, 0.5

$MgCl_2 \cdot 6H20$, 0.5 $Na_2H_2PO_4$, 5 $NaHCO_3$ and 1.5 $CaCl_2$ (pH 7.4 with NaOH). Amphotericin B (final concentration of 25 mg/mL, Sigma-Aldrich) was added to the pipette solution to give electrical access to the cells (series resistance of <100 MΩ). Alpha-cells in *Gcg*-GCaMP3 islets were confirmed by the presence of GCaMP3.

The frequency of action potential firing was calculated in MATLAB v. 6.1 (2000; The MathWorks, Natick, MA). In brief, a peak-find algorithm was used to detect action potentials. This was then used to calculate firing frequency in different experimental conditions (AVP concentrations). Power-spectrum analysis of V_M was conducted in Spike2 (CED, Cambridge, UK). V_M was moving-average filtered (interval of 200 ms) and the mean V_M subtracted. A power-spectrum was then produced (Hanning window with 0.15 Hz resolution) during 3 mM glucose alone, and with 10 pM AVP.

GCaMP3 imaging in mouse islets

Time-lapse imaging of the intracellular Ca^{2+} concentration ($[Ca^{2+}]_i$) in *Gcg*-GCaMP3 mouse islets was performed on an inverted Zeiss AxioVert 200 microscope, equipped with the Zeiss LSM 510-META laser confocal scanning system, using a 403/1.3 NA objective. Mouse islets were transferred into a custom-built recording chamber. Islets were then continuously perfused with bath solution at a rate of 200 µL/min. The bath solution contained (in mM): 140 NaCl, 5 KCl, 1.2 $MgCl_2$, 2.6 $CaCl_2$, 1 NaH_2PO_4, 10 Hepes, 17 mannitol and 3 glucose. GCaMP3 was excited at 430 nm and recorded at 300-530 nm. The pinhole diameter was kept constant, and frames of 256 x 256 pixels were taken every 800 ms. Unless otherwise stated, recordings were made in 3 mM glucose, to mimic hypoglycaemic conditions in mice. Raw GCaMP3 data was processed as follows; regions of interest (ROIs) were manually drawn around each $GCaMP3^+$ cell in ImageJ and the time-series of the GCaMP3 signal for each cell

was exported. These data were first imported into Spike2 7.04 (CED, Cambridge, UK), wherein the data was median filtered to remove baseline drift. The size of the filter was optimised for each individual cell to remove drift/artefacts but preserve Ca^{2+} transients. Ca^{2+} transients were then automatically detected using the built in peak-find algorithm; the amplitude of peaks to be detected was dependent on the SNR but was typically > 20% of the maximal signal intensity. Following this, frequency of Ca^{2+} transients could be determined. For plotting Ca^{2+} data, the data was imported into MATLAB.

DAG measurements in mouse islets

The effects of AVP on the intracellular diacylglycerol concentration (DAG) in pancreatic islet cells was studied using a recombinant circularly permutated probe, Upward DAG (Montana Molecular). Islets isolated from wild-type mice were gentle dispersed (using Trypsin ES) into clusters and platted on rectangular coverslips. Cell clusters were then transfected with Upward DAG, delivered via a BacMam infection (according to the manufacturer's guidelines). Coverslips were then were placed in a custom built chamber. Imaging experiments were performed 36-48 hours after infection using a Zeiss AxioZoom.V16 zoom microscope equipped with a ×2.3/0.57 objective (Carl Zeiss). The fluorescence was excited at 480 nm, and the emitted light was collected at 515 nm. The cells were kept at 33-35 °C and perfused continuously throughout the experiment with KRB solution supplemented with 3 mM glucose. The images were acquired using Zen Blue software (Carl Zeiss). The mean intensity for each cell was determined by manually drawing ROIs in ImageJ. Data analysis and representation was performed with MATLAB. All data was processed using a moving average filter function (*smooth*) with a span of 50 mins, minimum subtracted and then normalised to maximum signal intensity in the time-series. AUC was calculated using the *trapz* function and then divided by the length of the condition.

Ca^{2+} imaging in human islets

Time-lapse imaging of $[Ca^{2+}]_i$ in human islets was performed on the inverted Zeiss SteREO Discovery V20 Microscope, using a PlanApo S 3.5x mono objective. Human islets were loaded with 5 µg/µL of the Ca^{2+}-sensitive dye Fluo-4 (1923626, Invitrogen, Thermo Fisher Scientific) for 60 min before being transferred to a recording chamber. Islets were then continuously perfused with DMEM (11885-084, Gico, Thermo Fisher Scientific) with 10% FBS, 100 units/mL penicillin and 100 mg/mL streptomycin at a rate of 200 µL/min. Fluo-4 was excited at 488 nm and fluorescence emission collected at 530 nm. The pinhole diameter was kept constant, and frames of 1388x1040 pixels were taken every 3 sec. The mean intensity for each islet was determined by manually drawing an ROI around the islet in ImageJ. Data analysis and representation was performed with MATLAB. All data was processed using a moving average filter function (*smooth*) with a span of 20 mins, minimum subtracted and then normalised to maximum signal intensity in the time-series. AUC was calculated using the *trapz* function and then divided by the length of the condition.

Pancreatic islet isolation, transplantation and *in vivo* imaging of islets implanted into the anterior chamber of the eye (ACE).

Pancreatic islets from *Gcg*-GCaMP3 mice were isolated and cultured as described above. For transplantation, 10-20 islets were aspirated with a 27-gauge blunt eye cannula (BeaverVisitec, UK) connected to a 100 µl Hamilton syringe (Hamilton) via 0.4-mm polyethylene tubing (Portex Limited). Prior to surgery, mice (C57BL6/J) were anaesthetised with 2-4% isoflurane (Zoetis) and placed in a stereotactic frame. The cornea was incised near the junction with the sclera, then the blunt cannula (pre-loaded with islets) was inserted into the ACE and islets were expelled (average injection volume 20 µl for 10 islets). Carprofen

(Bayer, UK) and eye ointment were administered post-surgery. A minimum of four weeks was allowed for full implantation before imaging. Imaging sessions were performed with the mouse held in a stereotactic frame and the eye gently retracted, with the animal maintained under 2-4% isoflurane anaesthesia. All imaging experiments were conducted using a spinning disk confocal microscope (Nikon Eclipse Ti, Crest spinning disk, 20x water dipping 1.0 NA objective). The signal from GCaMP3 (ex. 488 nm, em. 525±25 nm) was monitored at 3 Hz for up to 20 min. After a baseline recording, mice received a bolus of AVP (10 µg/kg) i.v. (tail vein). Data were imported into ImageJ for initial movement correction (conducted with the StackReg and TurboReg plugins) and ROI selection. Analysis was then conducted in MATLAB.

Hormone secretion measurements from mouse and human islets

Islets, from human donors or isolated from wild-type mice, were incubated for 1 h in RPMI or DMEM supplemented with 7.5 mM glucose in a cell culture incubator. Size-matched batches of 15-20 islets were pre-incubated in 0.2 ml KRB with 2 mg/ml BSA (S6003, Sigma-Aldrich) and 3 mM glucose for 1 hour in a water-bath at 37 ^{0}C. Following this islets were statically subjected to 0.2 ml KRB with 2 mg/ml BSA with the condition (e.g. 10 pM AVP) for 1 hour. After each incubation, the supernatant was removed and kept, and 0.1 ml of acid:etoh (1:15) was added to the islets. Both of these were then stored at -80 ^{0}C. Each condition was repeated in at least triplicates.

Glucagon and insulin measurements in supernatants and content measurements were performed using a dual mouse insulin/glucagon assay system (Meso Scale Discovery, MD, U.S.A.) according to the protocol provided.

Hormone secretion measurements in the perfused mouse pancreas

Dynamic measurements of glucagon were performed using the *in situ* perfused mouse pancreas. Briefly, the aorta was cannulated by ligating above the coeliac artery and below the superior mesenteric artery, and the pancreas was perfused with KRB at a rate of ~0.45ml/min using an Ismatec Reglo Digital MS2/12 peristaltic pump. The KRB solution was maintained at 37 ^{0}C with a Warner Instruments temperature control unit TC-32 4B in conjunction with a tube heater (Warner Instruments P/N 64-0102) and a Harvard Apparatus heated rodent operating table. The effluent was collected by cannulating the portal vein and using a Teledyne ISCO Foxy R1 fraction collector. The pancreas was first perfused for 10 min with 3 mM glucose before commencing the experiment to establish the basal rate of secretion. Glucagon measurements in collected effluent were performed using RIA.

Flow cytometry of islet cells (FACS), RNA extraction, cDNA synthesis and quantitative PCR

The expression of the AVPR gene family was analysed in tissues from 12-week old C57BL6/J mice (3 mice) and pancreatic islets from human donors (2 samples, each comprised of pooled islet cDNA from 7 and 8 donors, respectively). Total RNA was isolated using a combination of TRIzol and PureLink RNA Mini Kit (Ambion, Thermofisher Scientific) with incorporated DNase treatment.

Pancreatic islets from *Gcg*-RFP mice were isolated and then dissociated into single cells by trypsin digestion and mechanical dissociation. Single cells were passed through a MoFlo Legacy (Beckman Coulter). Cells were purified by combining several narrow gates. Forward and side scatter were used to isolate small cells and to exclude cell debris. Cells were then gated on pulse width to exclude doublets or triplets. RFP^{+} cells were excited with a 488 nm

laser and the fluorescent signal was detected through a 580/30 bandpass filter (*i.e*. in the range 565-595 nm). RFP-negative cells were collected in parallel. The levels of gene expression in the RFP^+ and in the RFP^- FAC-sorted fractions were determined using real-time quantitative PCR (qPCR). RNA from FACS-sorted islet cells was isolated using RNeasy Micro Kit (Qiagen). cDNA was synthesized using the High Capacity RNA-to-cDNA kit (Applied Biosystems, Thermofisher Scientific). Real time qPCR was performed using SYBR Green detection and gene specific QuantiTect Primer Assays (Qiagen) on a 7900HT Applied Biosystems analyser. All reactions were run in triplicates. Relative expression was calculated using ΔCt method *Actb* as a reference gene.

Stereotaxic surgery and viral injections

For viral injections into the SON, mice were anaesthetized with ketamine/xylazine (100 and 10 mg/kg, respectively, i.p.) and then placed in a stereotaxic apparatus (David Kopf model 940). A pulled glass micropipette (20-40 μm diameter tip) was used for stereotaxic injections of adeno-associated virus (AAV). Virus was injected into the SON (200 nl/side; AP: −0.65 mm; ML: ±1.25 mm; DV: -5.4 mm from bregma) by an air pressure system using picoliter air puffs through a solenoid valve (Clippard EV 24VDC) pulsed by a Grass S48 stimulator to control injection speed (40 nL/min). The pipette was removed 3 min post-injection followed by wound closure using tissue adhesive (3M Vetbond). For viral injections into the VLM, mice were placed into a stereotaxic apparatus with the head angled down at approximately 45°. An incision was made at the level of the cisterna magna, then skin and muscle were retracted to expose the dura mater covering the 4th ventricle. A 28-gauge needle was used to make an incision in the dura and allow access to the VLM. Virus was then injected into the VLM (50nl*2/side; AP: -0.3 and -0.6mm; ML: ±1.3mm; DV: -1.7mm from obex) as described above. The pipette was removed 3 min post-injection followed by wound closure

using absorbable suture for muscle and silk suture for skin. For fibre photometry, an optic fibre (200 µm diameter, NA=0.39, metal ferrule, Thorlabs) was implanted in the SON and secured to the skull with dental cement. Subcutaneous injection of sustained release Meloxicam (4 mg/kg) was provided as postoperative care. The mouse was kept in a warm environment and closely monitored until resuming normal activity. Chemogenetic experiments utilized AAV8-hSyn-DIO-hM3Dq-mCherry (Addgene:44361) and AAV8-nEF-fDIO-hM4Di-mCherry (custom-made vector) produced from Boston Children's Hospital Viral Core and AAV5-EF1α-DIO-mCherry purchased from the UNC Vector Core. Fibre photometry experiments were conducted using AAV1-hSyn-FLEX-GCaMP6s purchased from the University of Pennsylvania (School of Medicine Vector Core). Projection mapping and ChR2-assisted circuit mapping were done using AAV9-EF1α-DIO-ChR2(H134R)-mCherry purchased from the University of Pennsylvania (School of Medicine Vector Core).

Fibre photometry experiments and analysis of photometry data.

In vivo fibre photometry was conducted as previously described (Mandelblat-Cerf *et al.* (2017)). A fibre optic cable (1-m long, metal ferrule, 400 µm diameter; Doric Lenses) was attached to the implanted optic cannula with zirconia sleeves (Doric Lenses). Laser light (473 nm) was focused on the opposite end of the fibre optic cable to titrate the light intensity entering the brain to 0.1-0.2 mW. Emitted light was passed through a dichroic mirror (Di02-R488-25x36, Semrock) and GFP emission filter (FF03-525/50-25, Semrock), before being focused onto a sensitive photodetector (Newport part #2151). The GCaMP6 signal was passed through a low-pass filter (50 Hz), and digitized at 1 KHz using a National Instruments data acquisition card and MATLAB software.

All experiments were conducted in the home-cage in freely moving mice. Animals prepared for *in vivo* fibre photometry experiments (outlined above), were subjected to an ITT or 2DG injection after overnight fasting. Prior to insulin or 2DG injection, a period of GCaMP6s activity was recorded (3 min) to establish baseline activity. Insulin (i.p. 2 U/kg), 2DG (i.p. 500mg/kg), or saline vehicle was then administered, and GCaMP6 activity recorded for a further 40 min. In some experiments, mice were pre-treated i.p. with CNO (1mg/kg) or saline, 30 minutes prior to insulin or 2DG. The recorded data was exported and then imported into MATLAB for analysis. Fluorescent traces were down-sampled to 1 Hz and the signal was normalised to the baseline (F_0 mean activity during baseline activity), with 100% signal being defined as the maximum signal in the entire trace (excluding the injection artefact). Following the ITT, the signal was binned (1 min) and a mean for each bin calculated. These binned signals were compared to baseline signal using a one-way RM ANOVA.

Surgery for continuous glucose monitoring

Animals that have undergone fibre photometry surgeries (3 weeks prior) were anesthetized and maintained with isoflurane. Once mice were fully anesthetized, the ventral abdomen and underside of the neck were shaved and disinfected. Animals were placed on their backs on a heated surgical surface. For transmitter implantation, a ventral midline abdomen incision was made and the abdominal wall was incised. The transmitter was placed in the abdominal cavity with the lead exiting cranially and the sensor and connector board exteriorized. The incision was sutured incorporating the suture rib into the closure. For glucose probe implantation, a midline neck incision was performed and the left common carotid artery was isolated. The vessel was then perforated and the sensor of the glucose probe (HD-XG, Data Sciences International) was advanced into the artery towards the heart, within a final placement in the aortic arch. Once in place, the catheter was secured by tying the suture

around the catheter and vessel, and overlying opening in tissue was closed. Mice were kept warm on a heating pad and monitored closely until fully recovered from anaesthesia.

Simultaneous AVP fiber photometry and continuous glucose monitoring

All experiments were conducted in the home-cage in freely moving mice. Animals prepared for in vivo fibre photometry and continuous glucose monitoring (outlined above), were subjected to an ITT after overnight fasting. After establishing > 3 min of baseline activity, insulin (i.p. 1 or 1.5 U/kg) or saline vehicle was administered. GCaMP6s activity, blood glucose, and body temperature were recorded throughout 2 h of experiment. Each recording was separated by at least 48h. GCaMP6s recording was performed as described above. Blood glucose and body temperature were acquired using Dataquest A.R.T. 4.36 system and analysed using MATLAB. Calibration of HD-XG device was performed as per manufacturer's manual.

In vivo measurements of plasma glucose, glucagon and copeptin

Samples for blood glucose and plasma glucagon measurements were taken from mice in response to different metabolic challenges (described in detail below). Both sexes were used for these experiments. Blood glucose was measured with an Accu-Chek Aviva (Roche Diagnostic, UK) and OneTouch Ultra (LifeScan, UK). Plasma copeptin was measured using an ELISA (MyBioSource, USA and Neo Scientific, USA).

Insulin tolerance test

Mice were restrained and a tail vein sample of blood was used to measure fed plasma glucose. A further sample was extracted into EDTA coated tubes for glucagon measurements. Aprotinin (1:5, 4 TIU/ml; Sigma-Aldrich, UK) was added to all blood samples. These blood

samples were kept on ice until the end of the experiment. Mice were first administered with any necessary pre-treatment and then individually caged. Pre-treatments included SSR149415 (30 mg/kg in PBS with 5% DMSO and 5% Cremophor EL), LY2409021 (5 mg/kg in PBS with 5% DMSO), CNO (1-3 mg/kg in PBS with 5% DMSO) or the appropriate vehicle. After a 30 minute period, mice were restrained again, and blood was taken via a tail vein or submandibular bleed. This was used for blood glucose measurements, and also for glucagon. Insulin (0.75, 1 or 1.5 U/kg) was then administered i.p., and the mice were re-caged. At regular time intervals after the insulin injection, mice were restrained and a blood sample extracted. Blood glucose was measured, and blood was taken for glucagon measurements. At the end of the experiment, blood samples were centrifuged at 2700 rpm for 10 min at 4 °C to obtain plasma. The plasma was then removed and stored at -80 °C. Plasma glucagon measurements were conducted using the 10-µl glucagon assay system (Mercodia, Upsala, Sweden), according to the manufacturer's protocol.

Fasting experiments

Wild-type mice were used for fasting experiments. Mice (8-9 weeks of age) were restrained, and blood was taken for blood glucose and glucagon measurements (as above). The mice were then home caged for the period of the fast. Food was removed at 08:30, and samples were taken at 14:30 and 16:00 (7.5 hour fast). SSR149415 (30 mg/kg) or vehicle was administered i.p. at 14:30 (90 minutes prior to termination of the fast). Blood glucagon was measured as indicated above. All animals had free access to water during the fast.

Water restriction (dehydration) experiments

Wild-type mice (8-9 weeks of age) were used for water restriction experiments. Mice were single housed one week prior to experimental manipulation. For trial 1 (water restriction),

blood was taken at 16:00 on day 1 and 2 for blood glucose and glucagon measurements (as above). Mice were water restricted for 24h between day 1 and 2, but had *ad lib* access to food. Amount of food consumed during this period was measured at the end of the trial and used for trial 2. For trial 2 (food restriction), blood was taken at 16:00 on day 1 and 2 for blood glucose and glucagon measurements. Mice had *ad lib* access to water between day 1 and 2, but were given the same amount of food consumed in trial 1. The two trials were separated by 2 days without any manipulation.

Glucoprivic response to 2-Deoxy-D-glucose

Wild-type mice were used for 2-Deoxy-D-glucose (2DG) experiments. The mice were single housed one week prior to experimental manipulation. On the experimental day, food was removed 4 hours prior to the experiment. 2DG (500 mg/kg) or saline vehicle was then administered i.p., and blood samples taken at regular intervals for blood glucose and plasma glucagon measurements. In some cohorts, the V1bR antagonist SSR149415 (30 mg/kg in PBS with 5% DMSO and 5% Tween 80), glucagon receptor antagonist LY240901 (5 mg/kg in PBS with 5% DMSO and 5% Tween 80) or appropriate vehicle was administered i.p. 30 minutes prior to administration of 2DG. Plasma glucagon was measured as described above.

Brain slice electrophysiology

To prepare brain slices for electrophysiological recordings, brains were removed from anesthetized mice (4–8 weeks old) and immediately placed in ice-cold cutting solution consisting of (in mM): 72 sucrose, 83 NaCl, 2.5 KCl, 1 NaH_2PO_4, 26 $NaHCO_3$, 22 glucose, 5 $MgCl_2$, 1 $CaCl_2$, oxygenated with 95% O_2 /5% CO_2 , measured osmolarity 310-320 mOsm/l. Cutting solution was prepared and used within 72 hours. 250 μm-thick coronal sections containing the PVH and SON were cut with a vibratome (7000smz2-Campden Instruments)

and incubated in oxygenated cutting solution at 34 °C for 25 min. Slices were transferred to oxygenated aCSF (126 mM NaCl, 21.4 mM $NaHCO_3$, 2.5 mM KCl, 1.2 mM NaH_2PO_4, 1.2 mM $MgCl_2$, 2.4 mM $CaCl_2$, 10 mM glucose) and stored in the same solution at room temperature (20-24 °C) for at least 60 min prior to recording. A single slice was placed in the recording chamber where it was continuously super-fused at a rate of 3–4 ml per min with oxygenated aCSF. Neurons were visualized with an upright microscope equipped with infrared-differential interference contrast and fluorescence optics. Borosilicate glass microelectrodes (5–7 MΩ) were filled with internal solution. All recordings were made using Multiclamp 700B amplifier, and data was filtered at 2 kHz and digitized at 10 kHz. All analysis was conducted off-line in MATLAB.

Channelrhodopsin-2 assisted circuit mapping (CRACM) of connections from A1/C1 neurons to the SON

A Cre-dependent viral vector containing the light-gated ion channel channelrhodopsin-2 (AAV-DIO-ChR2-mCherry) was injected into the VLM (targeting A1/C1 neurons) of Avp^{GFP} x Th^{Cre+} mice (see Fig. 5a) as described above (see 'Stereotaxic surgery and viral injections'). Brain slices were prepared (as above) from these mice. The SON was located by using the bifurcation of the anterior and middle cerebral arteries on the ventral surface of the brain as a landmark. Sections of 250 µm thickness of the SON were then cut with a Leica VT1000S or Campden Instrument 7000smz-2 vibratome, and incubated in oxygenated aCSF (126 mM NaCl, 21.4 mM $NaHCO_3$, 2.5 mM KCl, 1.2 mM NaH_2PO_4, 1.2 mM $MgCl_2$, 2.4 mM $CaCl_2$, 10 mM glucose) at 34 °C for 25 min. Slices recovered for 1 hr at room temperature (20–24°C) prior to recording. Whole-cell voltage clamp recordings were obtained using a Cs-based internal solution containing (in mM): 135 $CsMeSO_3$, 10 HEPES, 1 EGTA, 4 $MgCl_2$, 4 Na_2-ATP, 0.4 Na_2-GTP, 10 Na_2-phosphocreatine (pH 7.3; 295 mOsm). To photostimulate

ChR2-positive A1/C1 fibres, an LED light source (473 nm) was used. The blue light was focused on to the back aperture of the microscope objective, producing a wide-field exposure around the recorded cell of 1 mW. The light power at the specimen was measured using an optical power meter PM100D (ThorLabs). The light output is controlled by a programmable pulse stimulator, Master-8 (AMPI Co. Israel) and the pClamp 10.2 software (AXON Instruments).

Activation of hM3Dq with CNO in AVP neurons

The modified human M3 muscarinic receptor hM3Dq (Alexander *et al.*, 2009) was expressed in AVP neurons by injecting a Cre-dependent virus containing hM3Dq (AAV-DIO-hM3Dq-mCherry) into the SON of mice bearing *Avp* promoter-driven Cre recombinase (*Avp*$^{ires\text{-}Cre+}$ mice; see Fig. 1a). The intracellular solution for current clamp recordings contained the following (in mM): 128 K gluconate, 10 KCl, 10 HEPES, 1 EGTA, 1 $MgCl_2$, 0.3 CaCl2, 5 Na2ATP, 0.3 NaGTP, adjusted to pH 7.3 with KOH.

Brain immunohistochemistry

Mice were terminally anesthetized with chloral hydrate (Sigma-Aldrich) and trans-cardially perfused with phosphate-buffered saline (PBS) followed by 10% neutral buffered formalin (Fisher Scientific). Brains were extracted, cryoprotected in 20% sucrose, sectioned coronally on a freezing sliding microtome (Leica Biosystems) at 40 μm thickness, and collected in two equal series. Brain sections were washed in 0.1 M PBS with Tween-20, pH 7.4 (PBST), blocked in 3% normal donkey serum/0.25% Triton X-100 in PBS for 1 h at room temperature and then incubated overnight at room temperature in blocking solution containing primary antiserum (rat anti-mCherry, Invitrogen M11217, 1:1,000; chicken anti-GFP, Life Technologies A10262, 1:1,000; rabbit anti-vasopressin, Sigma-Aldrich AB1565, 1:1,000;

rabbit anti-TH, Millipore AB152, 1:1,000). The next morning, sections were extensively washed in PBS and then incubated in Alexa-fluor secondary antibody (1:1000) for 2 h at room temperature. After several washes in PBS, sections were incubated in DAPI solution (1 µg/ml in PBS) for 30 min. Then, sections were mounted on gelatin-coated slides and fluorescence images were captured using an Olympus VS120 slide scanner.

Reagents

AVP, hydrocortisone and adrenaline were all from Sigma (Sigma-Aldrich, UK). The G_q inhibitor YM-254890 (Takasaki *et al.*, 2004) was from Wako-Chem (Wake Pure Chemical Corp). The selective V1bR antagonist SSR149415 (nelivaptan; Serradeil-Le Gal *et al.* (2002)) was from Tocris (Bio-Techne Ltd, UK). The glucagon receptor antagonist LY2409021 (adomeglivant; Kazda *et al.* (2016)) was from MedKoo Biosciences (USA).

Clamping studies in human participants

Clamping studies were conducted at Gentofte Hospital, University of Copenhagen. The studies were approved by the Scientific-Ethical Committee of the Capital Region of Denmark (registration no. H-D-2009-0078) and was conducted according to the principles of the Declaration of Helsinki (fifth revision, Edinburgh, 2000).

Comparison of copeptin in healthy subjects undergoing a hypoglycaemic and euglycaemic clamp

Samples from the "saline arm" from 10 male subjects enrolled in an ongoing, unpublished clinical trial (https://clinicaltrials.gov/ct2/show/NCT03954873) were used to compare copeptin secretion during euglycaemia and hypoglycaemia.

For the study, two cannulae were inserted bilaterally into the cubital veins for infusions and blood sampling, respectively. For the euglycaemic study, participants were monitored during fasting glucose levels. For the hypoglycaemic clamp, an intravenous insulin (Actrapid; Novo Nordisk, Bagsværd, Denmark) infusion was initiated at time 0 min to lower plasma glucose. Plasma glucose was measured bedside every 5 min and kept >2.2 mM. Arterialised venous blood was drawn at regular time intervals prior to and during insulin infusion.

Comparison of copeptin in subjects with T1DM and healthy controls

Samples from 20 male (N=10 control and N=10 T1DM patients) from the "saline arms" of two previously published studies (Christensen *et al.*, 2011; Christensen *et al.*, 2015) were used to compare copeptin secretion during a hypoglycaemic clamp between T1DM and control subjects. The samples from healthy individuals (Controls) were from Christensen *et al.* (2011). These 10 healthy male subjects were of age 23 ± 1 years, BMI 23 ± 0.5 kg/m^2 and HbA_{1c} 5.5 ± 0.1%. The T1DM patient samples were from (Christensen *et al.*, 2015). These patients were; C-peptide negative, age 26 ± 1 years, BMI 24 ± 0.5 kg/m^2, HbA_{1c} 7.3 ± 0.2%, positive islet cell and/or GAD-65 antibodies, treated with multiple doses of insulin (N = 9) or insulin pump (N = 1), without late diabetes complications, without hypoglycemia unawareness, and without residual β-cell function (i.e., C-peptide negative after a 5-g arginine stimulation test). For the study, a hypoglycaemic clamp was conducted as outlined above.

Measurement of copeptin, glucagon and AVP in human plasma

Copeptin in human plasma was analysed using the KRYPTOR compact PLUS (Brahms Instruments, Thermo Fisher, DE). Glucagon was measured using human glucagon ELISA from Mercodia. Plasma AVP was measured using a human AVP ELISA kit (Cusabio, China).

Statistical tests of data

All data are reported as mean ± SEM. Unless otherwise stated, N refers to the number of mice. Statistical significance was defined as $p < 0.05$. All statistical tests were conducted in Prism8 (GraphPad Software, San Diego, CA, USA). For two groupings, a t test was conducted with the appropriate post hoc test. For more than two groupings, a one-way ANOVA was conducted (repeated measures, if appropriate). If data were separated by two treatments/factors, then a two-way ANOVA was conducted. A repeated measures (RM) two-way ANOVA was used (if appropriate), and a mixed-models ANOVA was used in the event of a repeated measures with missing data.

Mathematical model of G_q-mediated Ca^{2+} oscillations

The mathematical model of the processes governing Ca^{2+} signalling in a single cell following activation of a metabotropic receptor (i.e. V1bR) is based on the formalism by Li and Rinzel (1994) and Lemon *et al.* (2003). The simulations were conducted in the open source package software XPPAUT (http://www.math.pitt.edu/~bard/xpp/xpp.html).

References

Alexander GM, Rogan SC, Abbas AI, Armbruster BN, Pei Y, Allen JA, Nonneman RJ, Hartmann J, Moy SS, Nicolelis MA, McNamara JO & Roth BL. (2009). Remote control of neuronal activity in transgenic mice expressing evolved G protein-coupled receptors. *Neuron* **63,** 27-39.

Andrew SF, Dinh TT & Ritter S. (2007). Localized glucoprivation of hindbrain sites elicits corticosterone and glucagon secretion. *Am J Physiol Regul Integr Comp Physiol* **292,** R1792-1798.

Antoni FA. (1993). Vasopressinergic control of pituitary adrenocorticotropin secretion comes of age. *Front Neuroendocrinol* **14,** 76-122.

Armbruster BN, Li X, Pausch MH, Herlitze S & Roth BL. (2007). Evolving the lock to fit the key to create a family of G protein-coupled receptors potently activated by an inert ligand. *Proc Natl Acad Sci U S A* **104,** 5163-5168.

Basco D, Zhang Q, Salehi A, Tarasov A, Dolci W, Herrera P, Spiliotis I, Berney X, Tarussio D, Rorsman P & Thorens B. (2018). alpha-cell glucokinase suppresses glucose-regulated glucagon secretion. *Nat Commun* **9,** 546.

Bourque CW. (2008). Central mechanisms of osmosensation and systemic osmoregulation. *Nat Rev Neurosci* **9,** 519-531.

Briant LJB, Reinbothe TM, Spiliotis I, Miranda C, Rodriguez B & Rorsman P. (2018). delta-cells and beta-cells are electrically coupled and regulate alpha-cell activity via somatostatin. *J Physiol* **596,** 197-215.

Buchanan TA, Cane P, Eng CC, Sipos GF & Lee C. (1991). Hypothermia Is Critical for Survival during Prolonged Insulin-Induced Hypoglycemia in Rats. *Metabolism-Clinical and Experimental* **40,** 330-334.

Christensen M, Calanna S, Sparre-Ulrich AH, Kristensen PL, Rosenkilde MM, Faber J, Purrello F, van Hall G, Holst JJ, Vilsboll T & Knop FK. (2015). Glucose-dependent insulinotropic polypeptide augments glucagon responses to hypoglycemia in type 1 diabetes. *Diabetes* **64,** 72-78.

Christensen M, Vedtofte L, Holst JJ, Vilsboll T & Knop FK. (2011). Glucose-dependent insulinotropic polypeptide: a bifunctional glucose-dependent regulator of glucagon and insulin secretion in humans. *Diabetes* **60,** 3103-3109.

Cryer PE. (1994). Banting Lecture. Hypoglycemia: the limiting factor in the management of IDDM. *Diabetes* **43,** 1378-1389.

Cryer PE. (2002). Hypoglycaemia: the limiting factor in the glycaemic management of Type I and Type II diabetes. *Diabetologia* **45,** 937-948.

Cryer PE. (2007). Hypoglycemia, functional brain failure, and brain death. *J Clin Invest* **117,** 868-870.

Diem P, Redmon JB, Abid M, Moran A, Sutherland DE, Halter JB & Robertson RP. (1990). Glucagon, catecholamine and pancreatic polypeptide secretion in type I diabetic recipients of pancreas allografts. *J Clin Invest* **86,** 2008-2013.

DiGruccio MR, Mawla AM, Donaldson CJ, Noguchi GM, Vaughan J, Cowing-Zitron C, van der Meulen T & Huising MO. (2016). Comprehensive alpha, beta and delta cell transcriptomes reveal that ghrelin selectively activates delta cells and promotes somatostatin release from pancreatic islets. *Mol Metab* **5,** 449-458.

Dunning BE, Moltz JH & Fawcett CP. (1984). Modulation of insulin and glucagon secretion from the perfused rat pancreas by the neurohypophysial hormones and by desamino-D-arginine vasopressin (DDAVP). *Peptides* **5,** 871-875.

Freinkel N, Metzger BE, Harris E, Robinson S & Mager M. (1972). The hypothermia of hypoglycemia. Studies with 2-deoxy-D-glucose in normal human subjects and mice. *N Engl J Med* **287,** 841-845.

Gao ZY, Drews G, Nenquin M, Plant TD & Henquin JC. (1990). Mechanisms of the stimulation of insulin release by arginine-vasopressin in normal mouse islets. *J Biol Chem* **265,** 15724-15730.

Gao ZY, Gerard M & Henquin JC. (1992). Glucose- and concentration-dependence of vasopressin-induced hormone release by mouse pancreatic islets. *Regul Pept* **38,** 89-98.

Garfield AS, Shah BP, Madara JC, Burke LK, Patterson CM, Flak J, Neve RL, Evans ML, Lowell BB, Myers MG, Jr. & Heisler LK. (2014). A parabrachial-hypothalamic cholecystokinin neurocircuit controls counterregulatory responses to hypoglycemia. *Cell Metab* **20,** 1030-1037.

Grazzini E, Lodboerer AM, Perez-Martin A, Joubert D & Guillon G. (1996). Molecular and functional characterization of V1b vasopressin receptor in rat adrenal medulla. *Endocrinology* **137,** 3906-3914.

Gylfe E. (2013). Glucose Control of Glucagon Secretion: There Is More to It Than K-ATP Channels. *Diabetes* **62,** 1391-1393.

Hems DA & Whitton PD. (1973). Stimulation by vasopressin of glycogen breakdown and gluconeogenesis in the perfused rat liver. *Biochem J* **136,** 705-709.

Kazda CM, Ding Y, Kelly RP, Garhyan P, Shi CX, Lim CN, Fu HD, Watson DE, Lewin AJ, Landschulz WH, Deeg MA, Moller DE & Hardy TA. (2016). Evaluation of Efficacy and Safety of the Glucagon Receptor Antagonist LY2409021 in Patients With Type 2 Diabetes: 12-and 24-Week Phase 2 Studies. Diabetes Care 2016;39:1241-1249. *Diabetes Care* **39,** E199-E200.

Kim J, Okamoto H, Huang Z, Anguiano G, Chen S, Liu Q, Cavino K, Xin Y, Na E, Hamid R, Lee J, Zambrowicz B, Unger R, Murphy AJ, Xu Y, Yancopoulos GD, Li WH & Gromada J. (2017). Amino Acid Transporter Slc38a5 Controls Glucagon Receptor Inhibition-Induced Pancreatic alpha Cell Hyperplasia in Mice. *Cell Metab* **25,** 1348-1361 e1348.

Lai BK, Chae H, Gomez-Ruiz A, Cheng PP, Gallo P, Antoine N, Beauloye C, Jonas JC, Seghers V, Seino S & Gilon P. (2018). Somatostatin Is Only Partly Required for the Glucagonostatic Effect of Glucose but Is Necessary for the Glucagonostatic Effect of K-ATP Channel Blockers. *Diabetes* **67,** 2239-2253.

Lamy CM, Sanno H, Labouebe G, Picard A, Magnan C, Chatton JY & Thorens B. (2014). Hypoglycemia-activated GLUT2 neurons of the nucleus tractus solitarius stimulate vagal activity and glucagon secretion. *Cell Metab* **19,** 527-538.

Lawlor N, Youn A, Kursawe R, Ucar D & Stitzel ML. (2017). Alpha TC1 and Beta-TC-6 genomic profiling uncovers both shared and distinct transcriptional regulatory features with their primary islet counterparts. *Sci Rep-Uk* **7**.

Lemon G, Gibson WG & Bennett MR. (2003). Metabotropic receptor activation, desensitization and sequestration-II: modelling the dynamics of the pleckstrin homology domain. *J Theor Biol* **223,** 113-129.

Li AJ, Wang Q & Ritter S. (2018). Selective Pharmacogenetic Activation of Catecholamine Subgroups in the Ventrolateral Medulla Elicits Key Glucoregulatory Responses. *Endocrinology* **159,** 341-355.

Li GD, Pralong WF, Pittet D, Mayr GW, Schlegel W & Wollheim CB. (1992). Inositol Tetrakisphosphate Isomers and Elevation of Cytosolic Ca2+ in Vasopressin-Stimulated Insulin-Secreting Rinm5f Cells. *Journal of Biological Chemistry* **267,** 4349-4356.

Li YX & Rinzel J. (1994). Equations for InsP3 receptor-mediated [Ca2+]i oscillations derived from a detailed kinetic model: a Hodgkin-Huxley like formalism. *J Theor Biol* **166,** 461-473.

Lolait SJ, Stewart LQ, Jessop DS, Young WS, 3rd & O'Carroll AM. (2007). The hypothalamic-pituitary-adrenal axis response to stress in mice lacking functional vasopressin V1b receptors. *Endocrinology* **148,** 849-856.

Madden CJ, Stocker SD & Sved AF. (2006). Attenuation of homeostatic responses to hypotension and glucoprivation after destruction of catecholaminergic rostral ventrolateral medulla neurons. *Am J Physiol Regul Integr Comp Physiol* **291,** R751-759.

Mandelblat-Cerf Y, Kim A, Burgess CR, Subramanian S, Tannous BA, Lowell BB & Andermann ML. (2017). Bidirectional Anticipation of Future Osmotic Challenges by Vasopressin Neurons. *Neuron* **93,** 57-65.

Marty N, Dallaporta M, Foretz M, Emery M, Tarussio D, Bady I, Binnert C, Beermann F & Thorens B. (2005). Regulation of glucagon secretion by glucose transporter type 2 (glut2) and astrocyte-dependent glucose sensors. *J Clin Invest* **115,** 3545-3553.

Marty N, Dallaporta M & Thorens B. (2007). Brain glucose sensing, counterregulation, and energy homeostasis. *Physiology (Bethesda)* **22,** 241-251.

Mawla AM & Huising MO. (2019). Navigating the Depths and Avoiding the Shallows of Pancreatic Islet Cell Transcriptomes. *Diabetes* **68,** 1380-1393.

McCrimmon RJ & Sherwin RS. (2010). Hypoglycemia in type 1 diabetes. *Diabetes* **59,** 2333-2339.

Meek TH, Nelson JT, Matsen ME, Dorfman MD, Guyenet SJ, Damian V, Allison MB, Scarlett JM, Nguyen HT, Thaler JP, Olson DP, Myers MG, Jr., Schwartz MW & Morton GJ. (2016). Functional identification of a neurocircuit regulating blood glucose. *Proc Natl Acad Sci U S A* **113,** E2073-2082.

Nica AC, Ongen H, Irminger JC, Bosco D, Berney T, Antonarakis SE, Halban PA & Dermitzakis ET. (2013). Cell-type, allelic, and genetic signatures in the human pancreatic beta cell transcriptome. *Genome Res* **23,** 1554-1562.

Niijima A. (1982). Glucose-sensitive afferent nerve fibres in the hepatic branch of the vagus nerve in the guinea-pig. *J Physiol* **332,** 315-323.

Pei H, Sutton AK, Burnett KH, Fuller PM & Olson DP. (2014). AVP neurons in the paraventricular nucleus of the hypothalamus regulate feeding. *Mol Metab* **3,** 209-215.

Petreanu L, Huber D, Sobczyk A & Svoboda K. (2007). Channelrhodopsin-2-assisted circuit mapping of long-range callosal projections. *Nat Neurosci* **10,** 663-668.

Ritter S, Dinh TT & Zhang Y. (2000). Localization of hindbrain glucoreceptive sites controlling food intake and blood glucose. *Brain Res* **856,** 37-47.

Rodriguez-Diaz R, Molano RD, Weitz JR, Abdulreda MH, Berman DM, Leibiger B, Leibiger IB, Kenyon NS, Ricordi C, Pileggi A, Caicedo A & Berggren PO. (2018). Paracrine Interactions within the Pancreatic Islet Determine the Glycemic Set Point. *Cell Metab* **27,** 549-+.

Rorsman P, Ramracheya R, Rorsman NJ & Zhang Q. (2014). ATP-regulated potassium channels and voltage-gated calcium channels in pancreatic alpha and beta cells: similar functions but reciprocal effects on secretion. *Diabetologia* **57,** 1749-1761.

Ross CA, Ruggiero DA, Park DH, Joh TH, Sved AF, Fernandez-Pardal J, Saavedra JM & Reis DJ. (1984). Tonic vasomotor control by the rostral ventrolateral medulla: effect of electrical or chemical stimulation of the area containing C1 adrenaline neurons on arterial pressure, heart rate, and plasma catecholamines and vasopressin. *J Neurosci* **4,** 474-494.

Salem V, Silva LD, Suba K, Georgiadou E, Gharavy SNM, Akhtar N, Martin-Alonso A, Gaboriau DCA, Rothery SM, Stylianides T, Carrat G, Pullen TJ, Singh SP, Hodson DJ, Leclerc I, Shapiro AMJ, Marchetti P, Briant LJB, Distaso W, Ninov N & Rutter GA. (2019). Leader beta-cells coordinate Ca2+ dynamics across pancreatic islets in vivo. *Nat Metab* **1,** 615-629.

Sawchenko PE & Swanson LW. (1983). The organization of forebrain afferents to the paraventricular and supraoptic nuclei of the rat. *J Comp Neurol* **218,** 121-144.

Schwartz MW, Seeley RJ, Tschop MH, Woods SC, Morton GJ, Myers MG & D'Alessio D. (2013). Cooperation between brain and islet in glucose homeostasis and diabetes. *Nature* **503,** 59-66.

Serradeil-Le Gal C, Wagnon J, Simiand J, Griebel G, Lacour C, Guillon G, Barberis C, Brossard G, Soubrie P, Nisato D, Pascal M, Pruss R, Scatton B, Maffrand JP & Le Fur G. (2002). Characterization of (2S,4R)-1-[5-chloro-1-[(2,4-dimethoxyphenyl)sulfonyl]-3-(2-methoxy-phenyl)-2-oxo- 2,3-dihydro-1H-indol-3-yl]-4-hydroxy-N,N-dimethyl-2-pyrrolidine carboxamide (SSR149415), a selective and orally active vasopressin V1b receptor antagonist. *J Pharmacol Exp Ther* **300,** 1122-1130.

Siafarikas A, Johnston RJ, Bulsara MK, O'Leary P, Jones TW & Davis EA. (2012). Early loss of the glucagon response to hypoglycemia in adolescents with type 1 diabetes. *Diabetes Care* **35,** 1757-1762.

Sloop KW, Cao JX, Siesky AM, Zhang HY, Bodenmiller DM, Cox AL, Jacobs SJ, Moyers JS, Owens RA, Showalter AD, Brenner MB, Raap A, Gromada J, Berridge BR, Monteith DK, Porksen N, McKay RA, Monia BP, Bhanot S, Watts LM & Michael MD. (2004). Hepatic and glucagon-like peptide-1-mediated reversal of diabetes by glucagon receptor antisense oligonucleotide inhibitors. *J Clin Invest* **113,** 1571-1581.

Svendsen B, Larsen O, Gabe MBN, Christiansen CB, Rosenkilde MM, Drucker DJ & Holst JJ. (2018). Insulin Secretion Depends on Intra-islet Glucagon Signaling. *Cell Rep* **25,** 1127-1134 e1122.

Takasaki J, Saito T, Taniguchi M, Kawasaki T, Moritani Y, Hayashi K & Kobori M. (2004). A novel Galphaq/11-selective inhibitor. *J Biol Chem* **279,** 47438-47445.

Taveau C, Chollet C, Bichet DG, Velho G, Guillon G, Corbani M, Roussel R, Bankir L, Melander O & Bouby N. (2017). Acute and chronic hyperglycemic effects of vasopressin in normal rats: involvement of V1A receptors. *Am J Physiol Endocrinol Metab* **312,** E127-E135.

Thorens B. (2014). Neural regulation of pancreatic islet cell mass and function. *Diabetes Obes Metab* **16 Suppl 1,** 87-95.

Unger RH & Cherrington AD. (2012). Glucagonocentric restructuring of diabetes: a pathophysiologic and therapeutic makeover. *J Clin Invest* **122,** 4-12.

van der Meulen T, Mawla AM, DiGruccio MR, Adams MW, Nies V, Dolleman S, Liu S, Ackermann AM, Caceres E, Hunter AE, Kaestner KH, Donaldson CJ & Huising MO. (2017). Virgin Beta Cells Persist throughout Life at a Neogenic Niche within Pancreatic Islets. *Cell Metab* **25,** 911-926 e916.

Verberne AJM, Sabetghadam A & Korim WS. (2014). Neural pathways that control the glucose counterregulatory response. *Front Neurosci-Switz* **8**.

Vergari E, Knudsen JG, Ramracheya R, Salehi A, Zhang Q, Adam J, Asterholm IW, Benrick A, Briant LJB, Chibalina MV, Gribble FM, Hamilton A, Hastoy B, Reimann F, Rorsman NJG, Spiliotis II, Tarasov A, Wu Y, Ashcroft FM & Rorsman P. (2019). Insulin inhibits glucagon release by SGLT2-induced stimulation of somatostatin secretion. *Nature Communications* **10,** 139.

Watts AG & Boyle CN. (2010). The functional architecture of dehydration-anorexia. *Physiol Behav* **100,** 472-477.

Wersinger SR, Ginns EI, O'Carroll AM, Lolait SJ & Young WS, 3rd. (2002). Vasopressin V1b receptor knockout reduces aggressive behavior in male mice. *Mol Psychiatry* **7,** 975-984.

Yibchok-Anun S, Cheng H, Chen TH & Hsu WH. (2000). Mechanisms of AVP-induced glucagon release in clonal alpha-cells in-R1-G9: involvement of Ca(2+)-dependent and -independent pathways. *Br J Pharmacol* **129,** 257-264.

Yu Q, Shuai H, Ahooghalandari P, Gylfe E & Tengholm A. (2019). Glucose controls glucagon secretion by directly modulating cAMP in alpha cells. *Diabetologia*.

Zhao Z, Wang L, Gao W, Hu F, Zhang J, Ren Y, Lin R, Feng Q, Cheng M, Ju D, Chi Q, Wang D, Song S, Luo M & Zhan C. (2017). A Central Catecholaminergic Circuit Controls Blood Glucose Levels during Stress. *Neuron* **95,** 138-152 e135.

Fig. 1

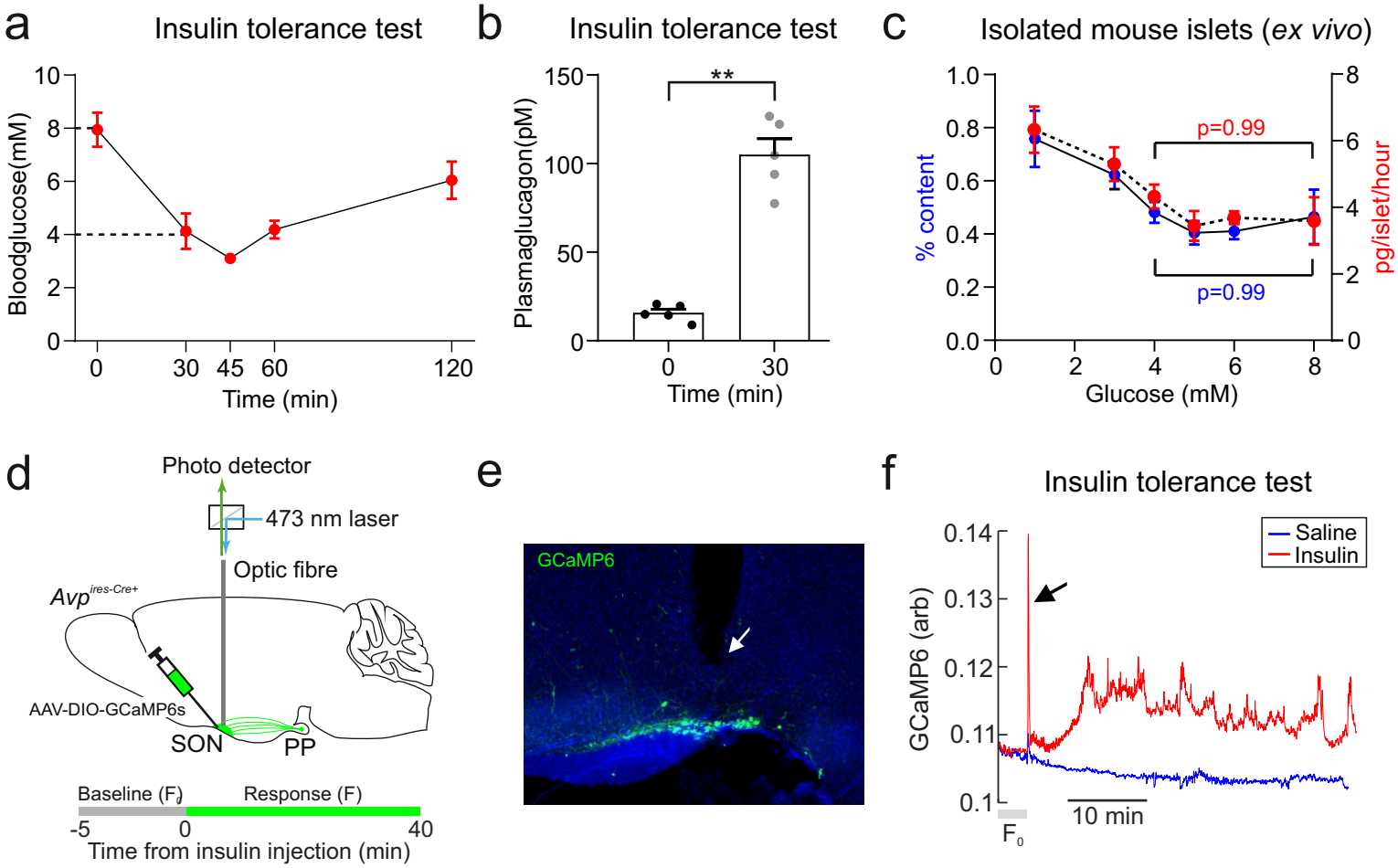

Fig. 2

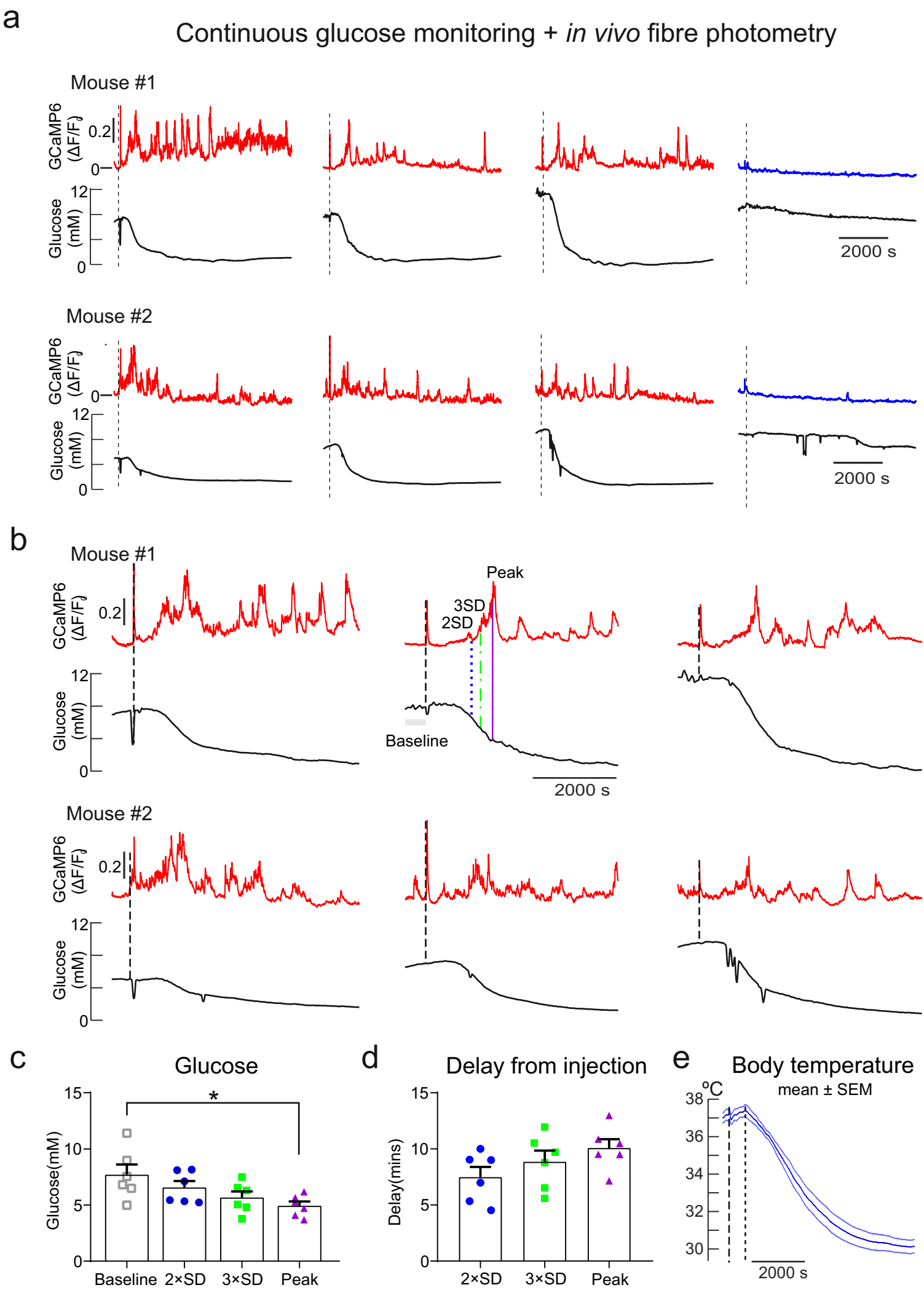

Fig. 3

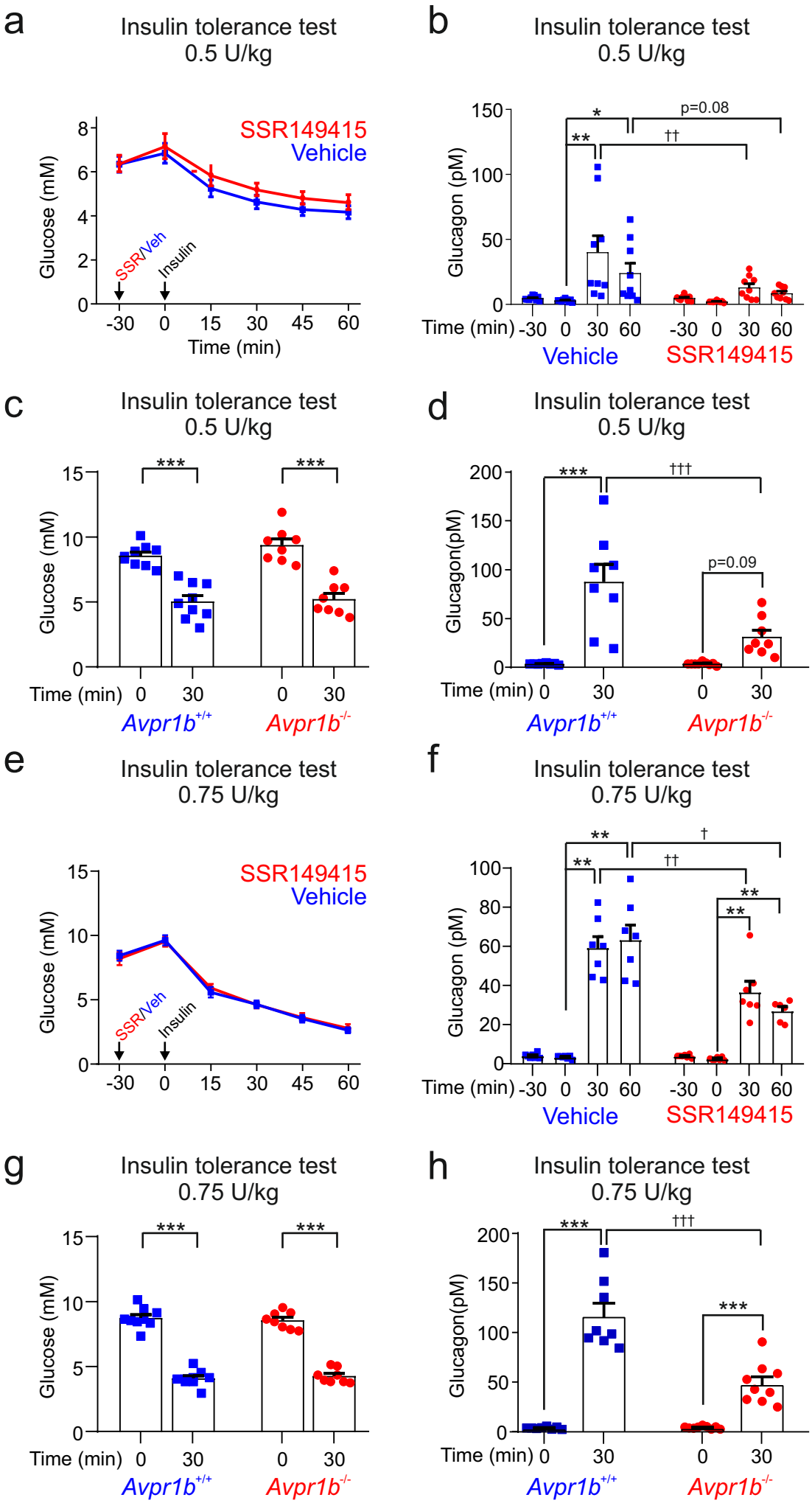

Fig. 4

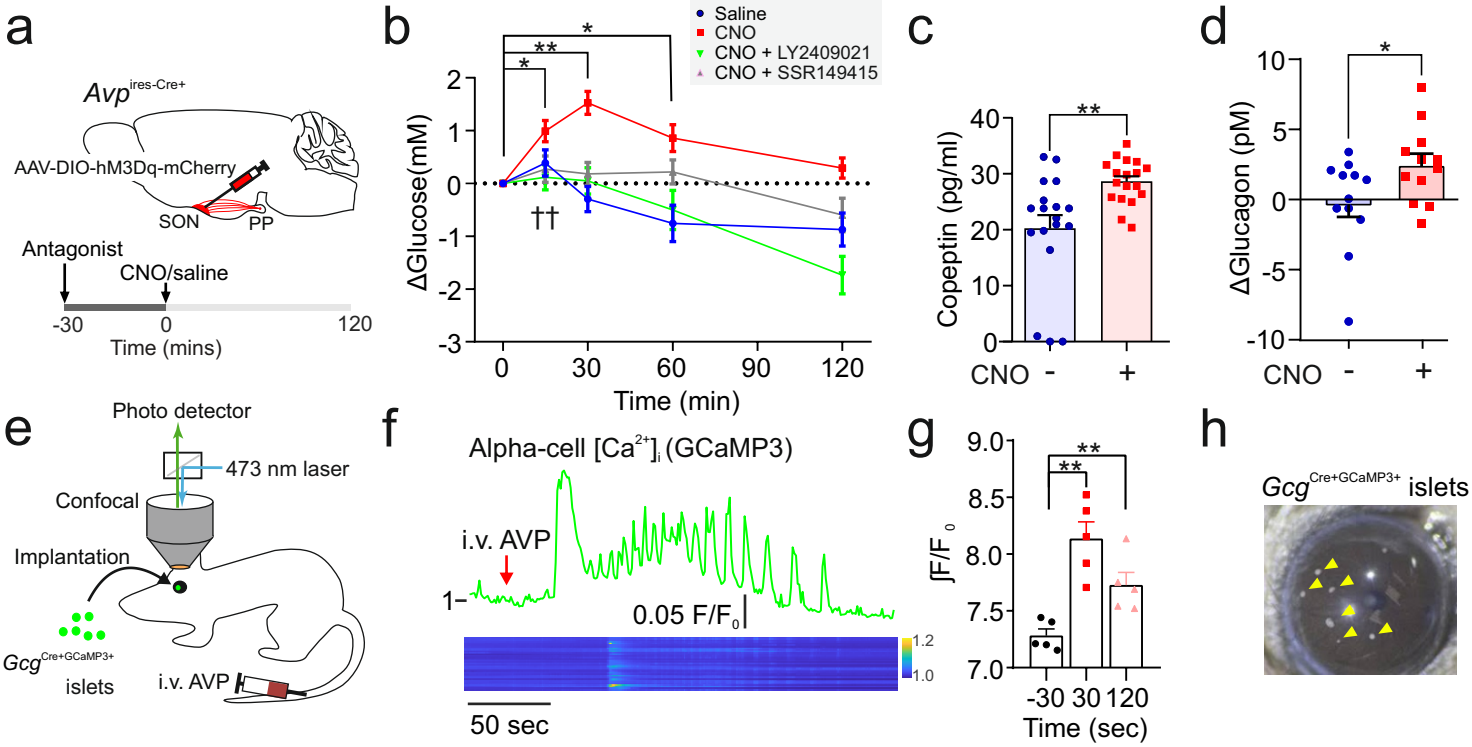

Fig. 5

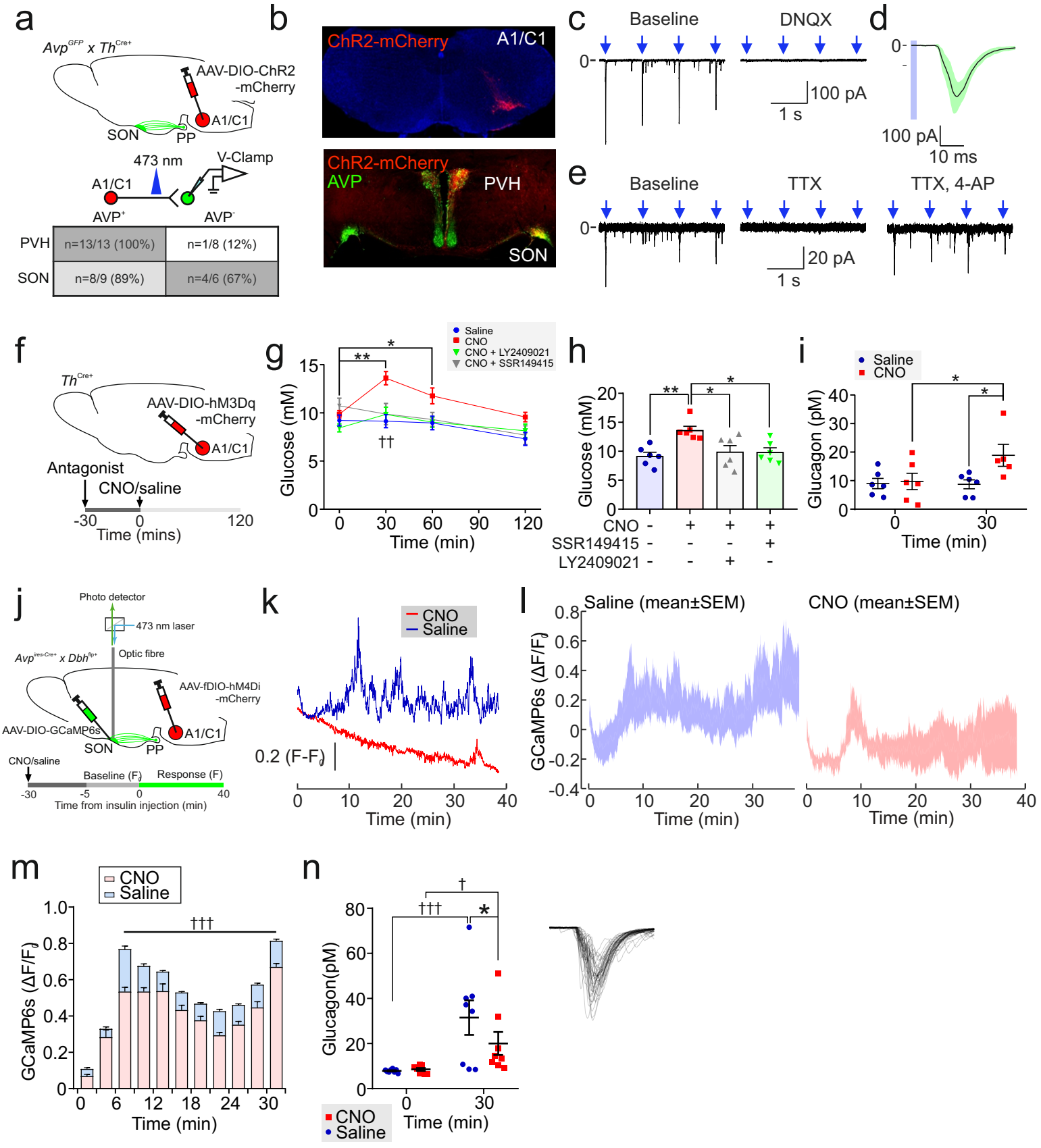

Fig. 6

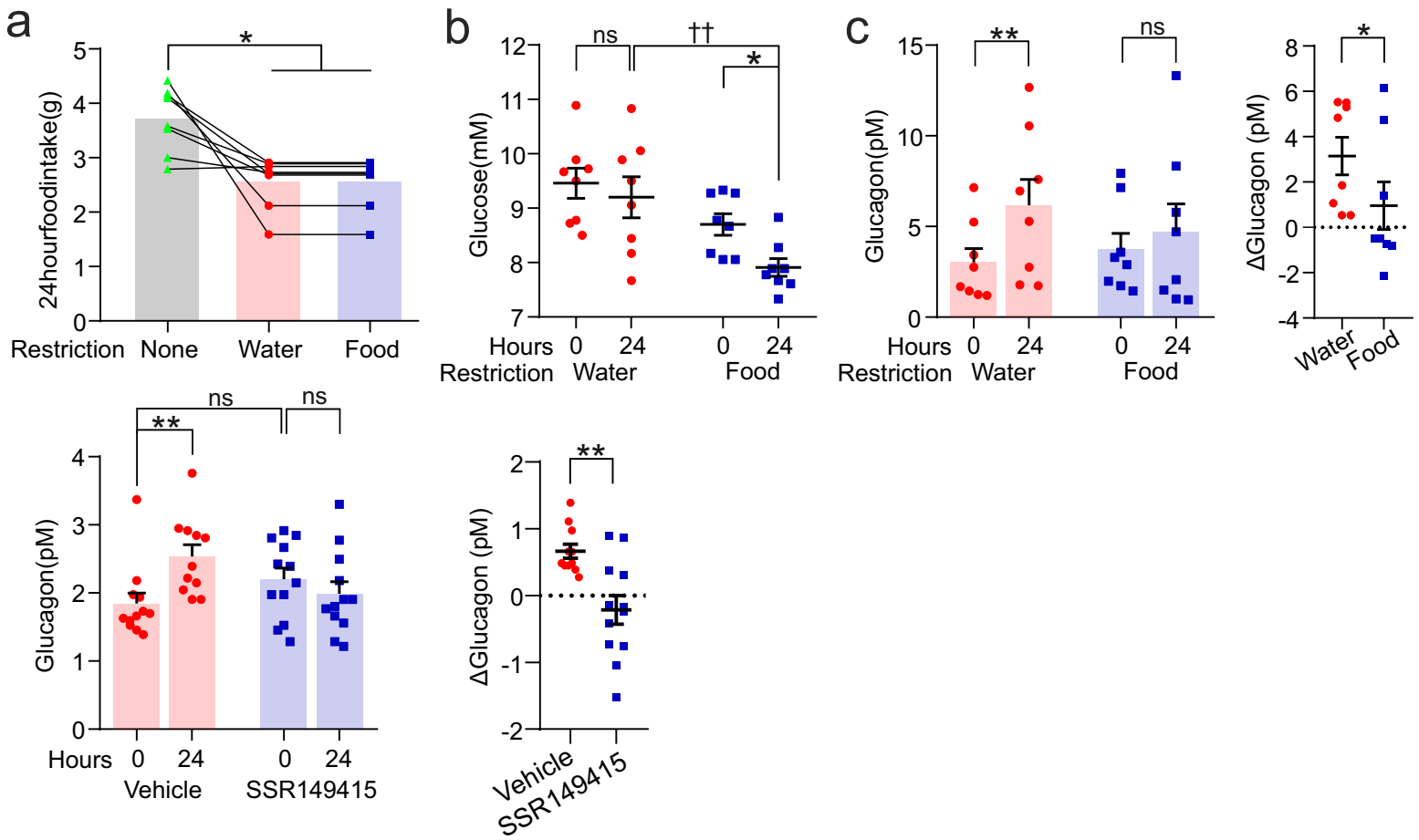

Fig. 7

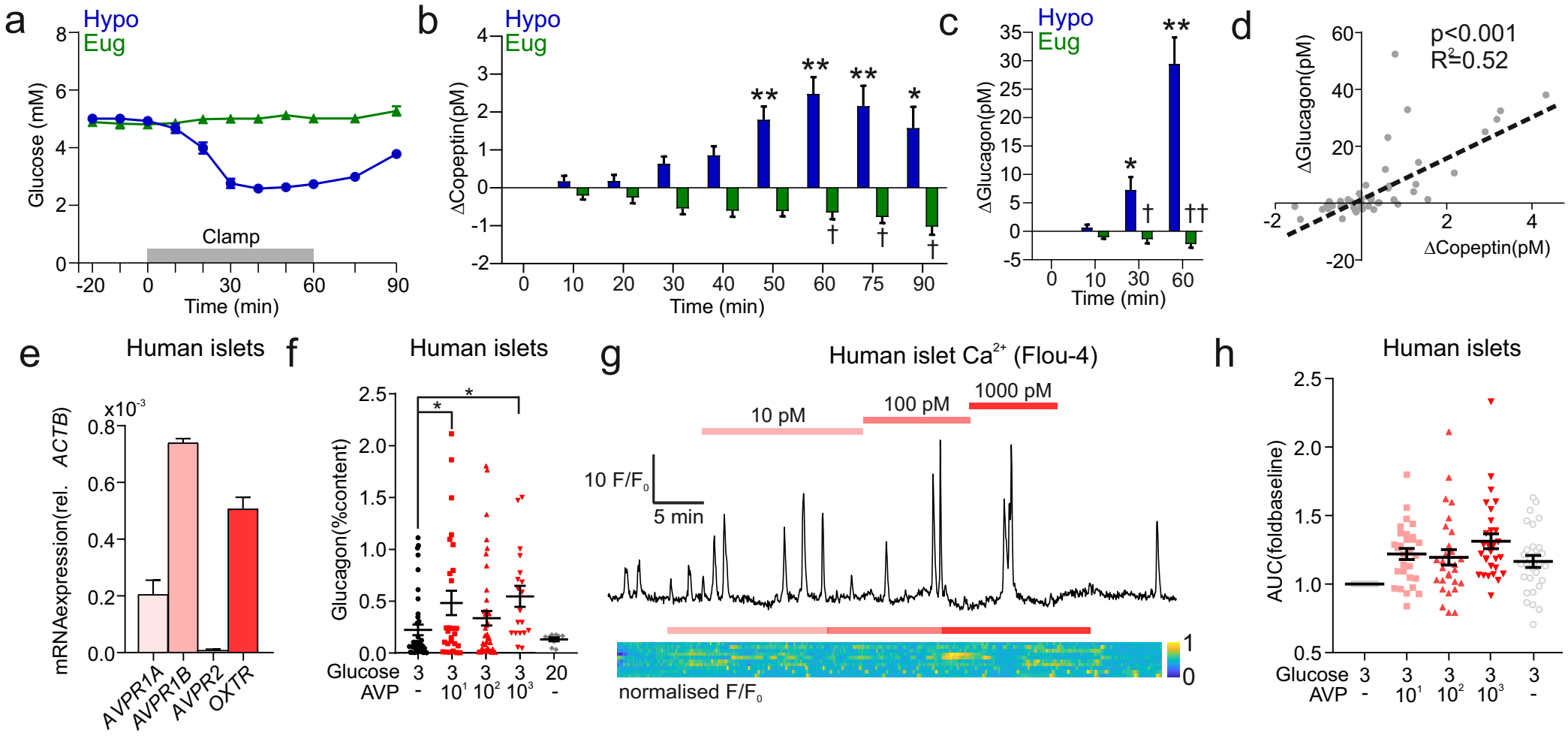
a
Hypo
Eug
Glucose (mM)
Clamp
Time (min)
b
Hypo
Eug
ΔCopeptin(pM)
Time (min)
c
Hypo
Eug
ΔGlucagon(pM)
Time (min)
d
p<0.001
R²=0.52
ΔGlucagon(pM)
ΔCopeptin(pM)
e
Human islets
x10⁻³
mRNAexpression(rel. ACTB)
AVPR1A
AVPR1B
AVPR2
OXTR
f
Human islets
Glucagon(%content)
Glucose
AVP
g
Human islet Ca²⁺ (Flou-4)
10 pM
100 pM
1000 pM
10 F/F₀
5 min
normalised F/F₀
h
Human islets
AUC(foldbaseline)
Glucose
AVP

Fig. 8

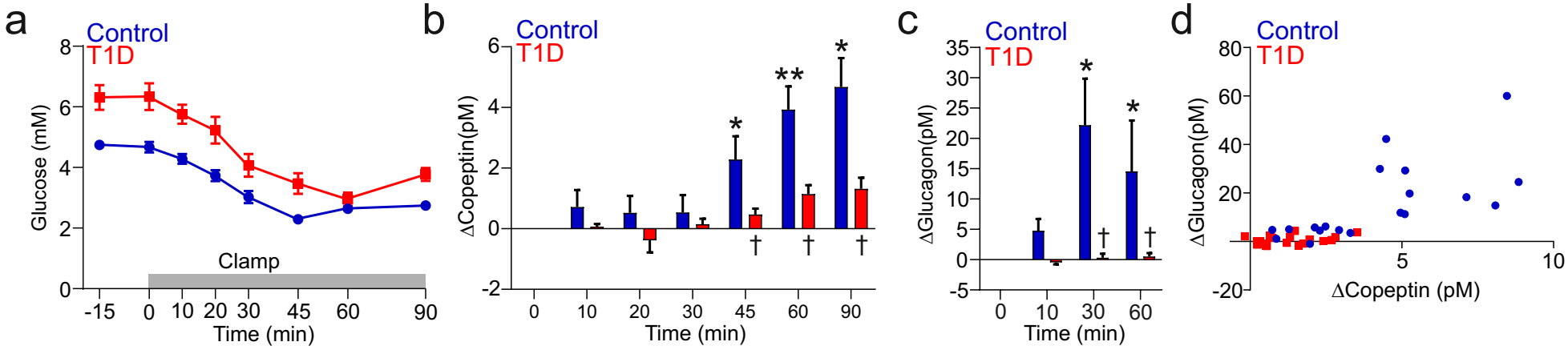
a
Control
T1D
Glucose (mM)
Clamp
Time (min)
b
Control
T1D
ΔCopeptin(pM)
Time (min)
c
Control
T1D
ΔGlucagon(pM)
Time (min)
d
Control
T1D
ΔGlucagon(pM)
ΔCopeptin (pM)

Supplementary Fig. 1

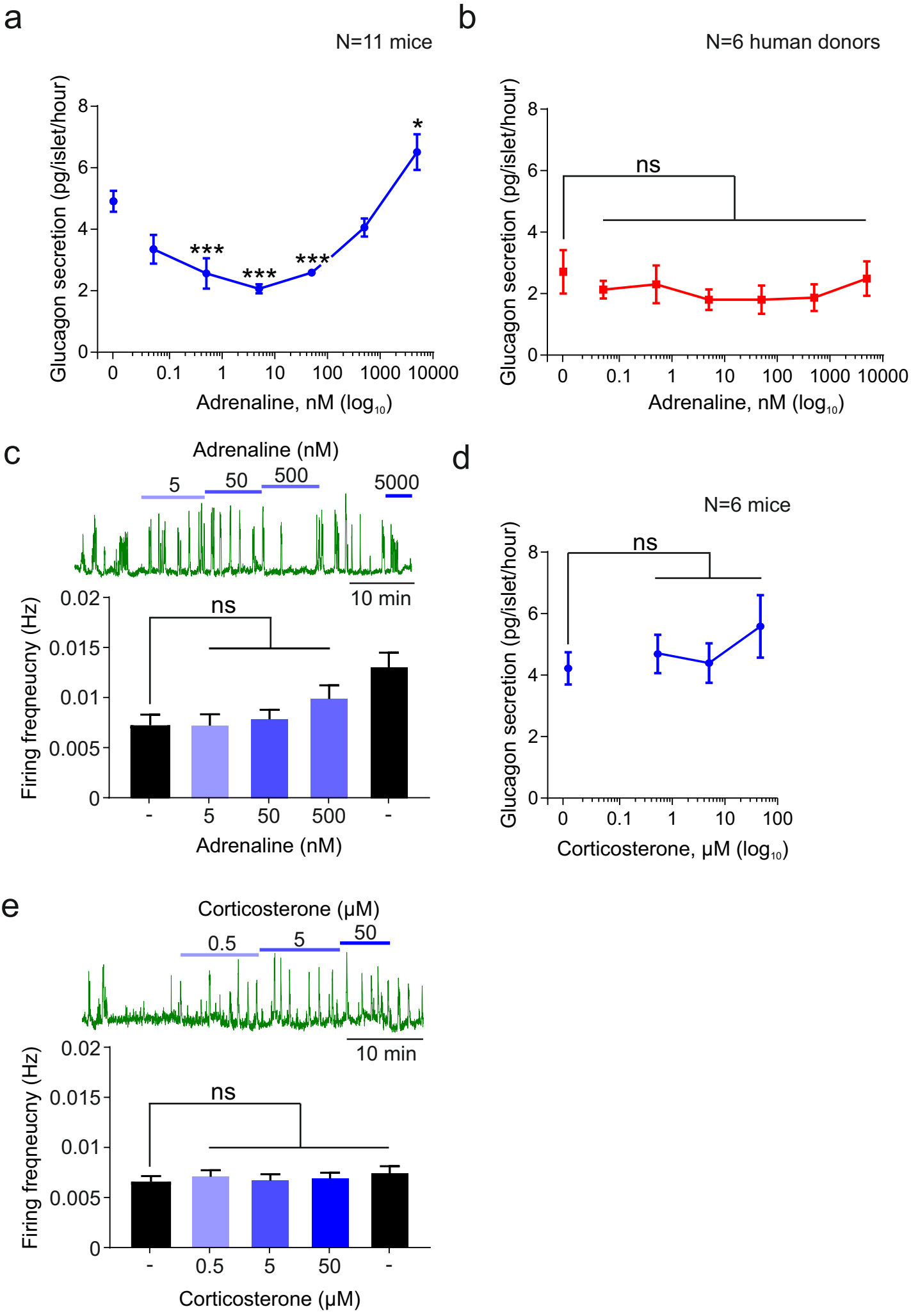

Supplementary Fig. 2

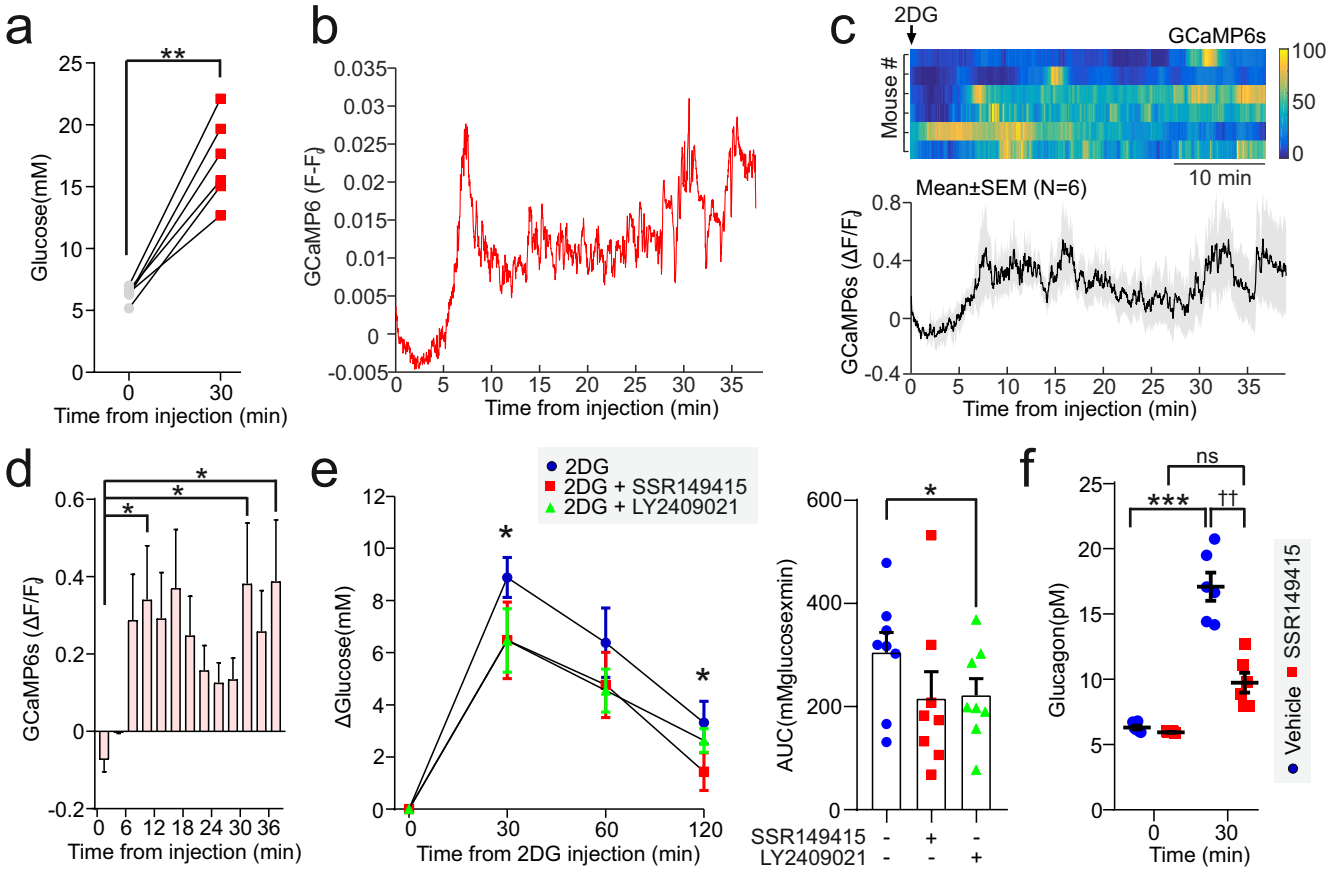

Supplementary Fig. 3

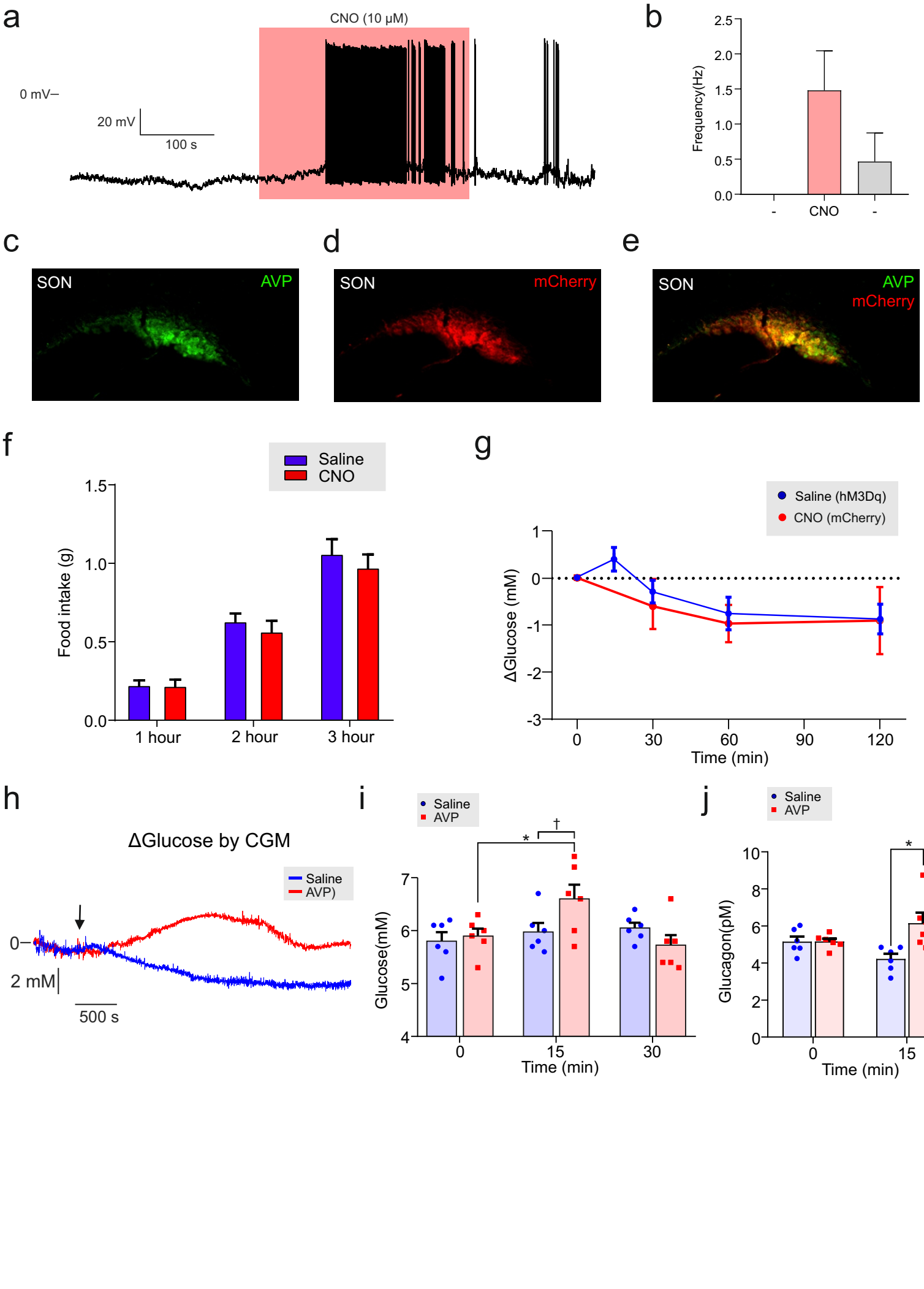

Supplementary Fig. 4

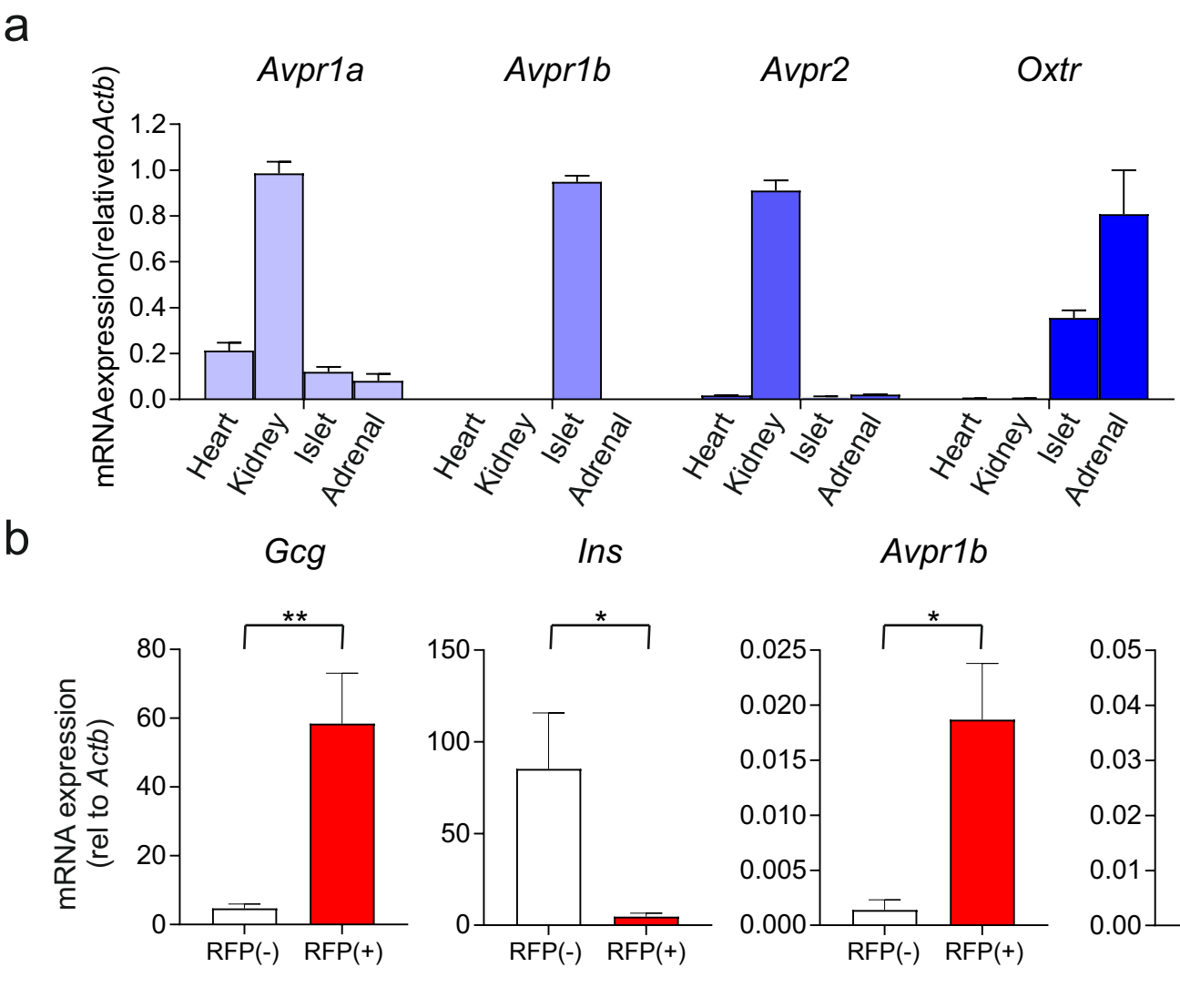

Supplementary Fig. 5

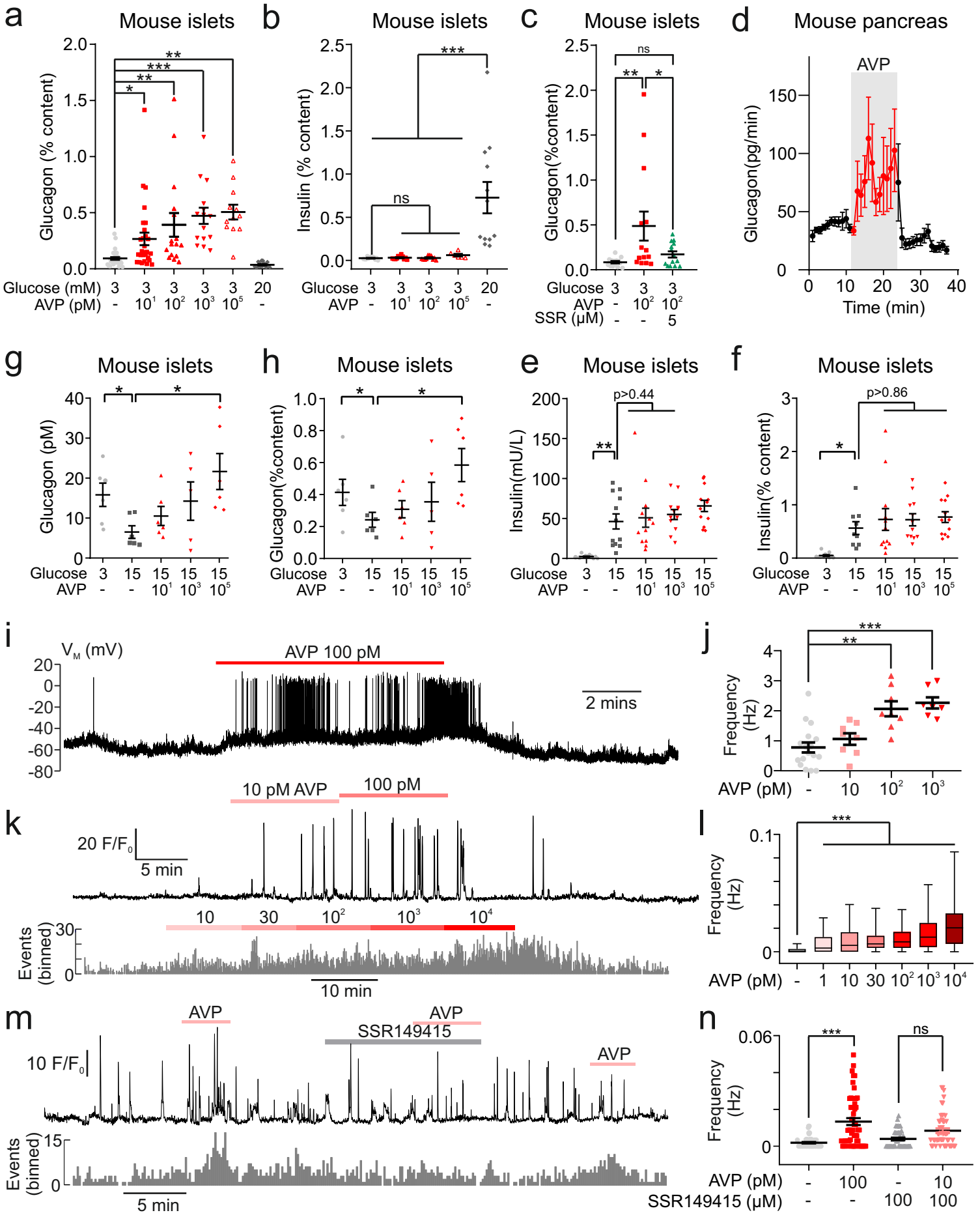

Supplementary Fig. 6

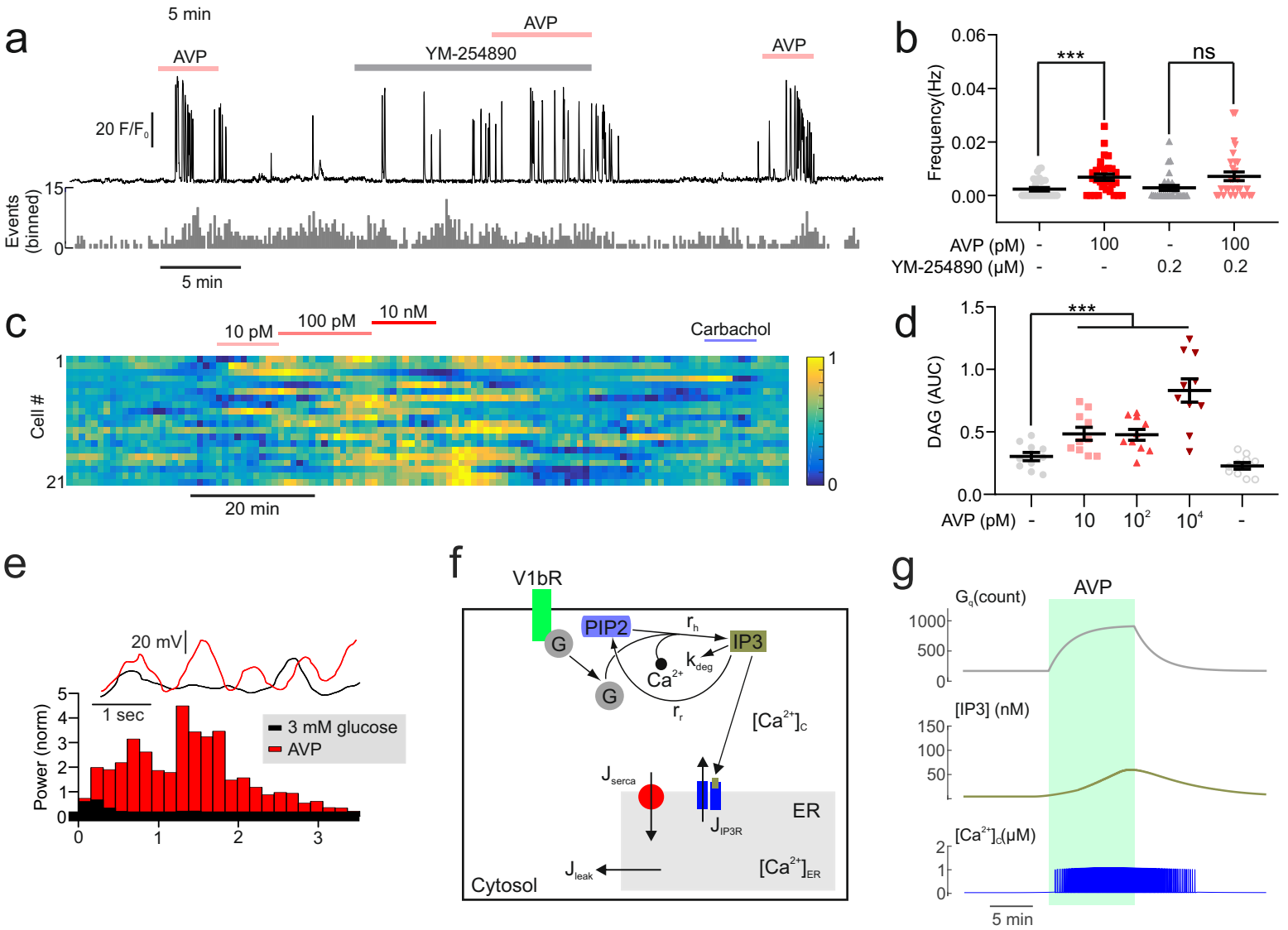

Supplementary Fig 7

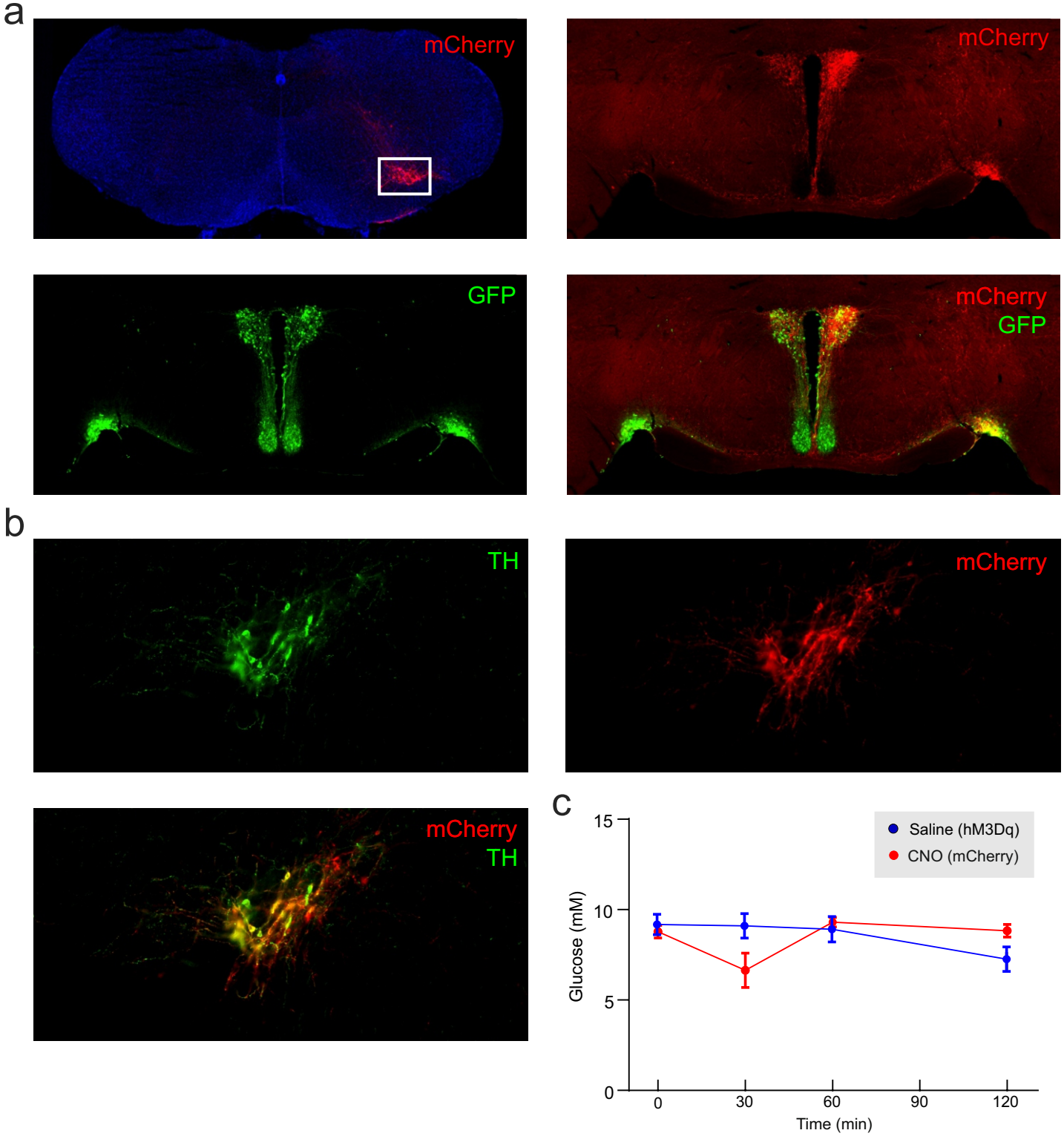

Supplementary Fig. 8

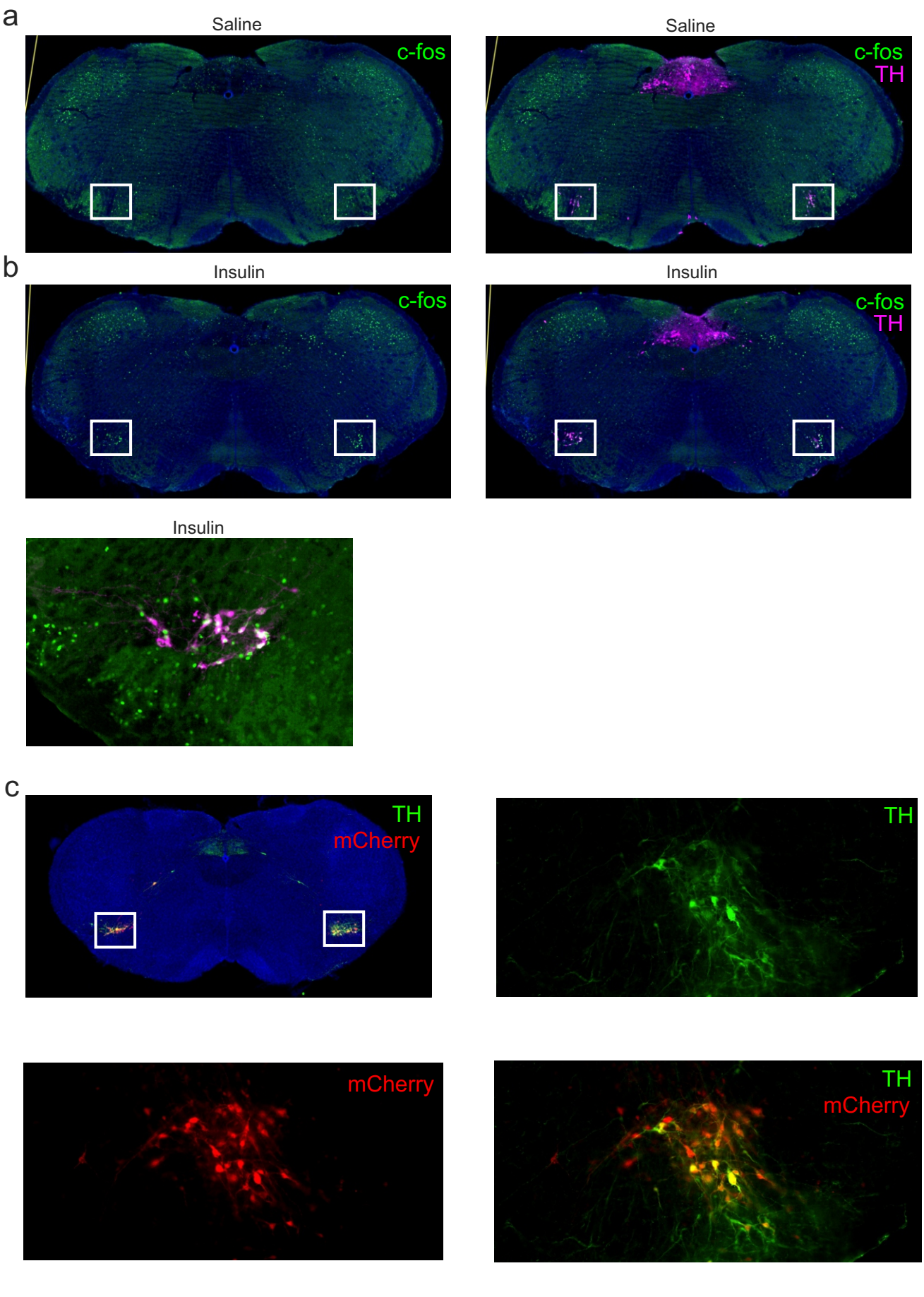

Supplementary Fig 9